## 5. Formulation, development and evaluation of CS encapsulated polymeric nanoparticles (CS-PNs)

### 5.1 Experimental methods

#### 5.1.1 Pre-formulation studies

Preformulation study is the first step in rational development of dosage form of any drug substance. It is the process of optimizing the delivery of drug by virtue of determining the physicochemical properties of the new compound that could affect drug performance for development of an efficacious, stable and safe dosage form [175]. The following studies were performed:

##### 5.1.1.1 Solubility study

Saturation solubility of CS was determined in distilled water and different buffer solutions as a function of pH at 25 ± 2 $^{o}$C by shake flask method [175, 176]. Different buffer solutions such as pH 1.2 (hydrochloric acid), pH 3.6, pH 4.9, pH 6.8 and pH 7.4 (phosphate) were chosen for the solubility study. Briefly, the excessive amount of CS was added in each six conical flasks containing 10 ml of different media. Each conical flask was tightly corked, placed in a rotary shaker at 25 ± 2 $^{o}$C and agitated at 100 rpm for 48 hr. In between, if CS was dissolved in any media then, extra CS was added to make solution saturated. After 48 hr, aliquots from each flask were separated and filtered through 0.45 μm filter. The filtered solutions were diluted with respective media and analyzed for solubilized drug content by UV-Visible spectrophotometer at 239 nm. Each solubility value was determined in triplicate (n=3) and the results were reported as mean ± standard deviation (SD).

### 5.1.1.2 Drug excipients compatibility studies

#### 5.1.1.2.1 Fourier transform infrared (FTIR) spectroscopy

FTIR spectroscopic study of CS, PLGA, PVA and their physical mixture was conducted using FTIR spectrophotometer (Shimadzu, Model-8400S, Japan) in order to assess the possibility of chemical interaction, if any, between CS and other excipients. Briefly, samples were homogeneously dispersed and triturated in glass mortar-pestle with dry, micronized potassium bromide (KBr). The sample mixture was then placed in an evacuable die and compressed to form thin, compact pellet using pressed pellet technique. Sample compressed pellets were placed in IR path length for scanning against the blank KBr pellet background, over the wavenumber ranging from 4000 $cm^{-1}$ to 400 $cm^{-1}$. FTIR spectra were collected after 20 scans, with a resolution of 4 $cm^{-1}$ at room temperature [23, 39].

#### 5.1.1.2.2 Differential scanning calorimetry (DSC) study

The thermal behaviour of CS, PLGA, PVA and their physical mixture was characterized by using TGA/DSC-1, Star® system (Mettler Toledo, Switzerland) with an auto cool accessory, for evaluating the compatibility of CS with other excipients. The instrument was previously calibrated with indium standard for baseline. The small amount of sample (approximately 3-5 mg) was hermetically sealed into an aluminum crimp cell and temperature was raised at a rate of 10 $^{o}$C/min over the scanning temperature range from 30 to 300 $^{o}$C under constant nitrogen atmosphere (purging rate of 10 ml/min), against an empty aluminum pan as a reference. The heat flow as a function of temperature was measured for each sample. The thermogram of pure CS was compared with the thermogram of physical mixture [23, 39].

### 5.1.2 Formulation of CS encapsulated polymeric nanoparticles

CS-PNs were prepared based on double emulsification solvent evaporation ($W_1/O/W_2$) method with suitable modifications [24]. Briefly, 0.5 ml of aqueous phase containing 25 mg of CS ($W_1$; internal aqueous phase) was emulsified with the predetermined amount of PLGA and Span 80 containing dichloromethane (DCM) (O; organic phase), with the help of ultra probe sonicator (UP50H, Hielscher, USA) for 90 sec at 80% sonication amplitude. This obtained primary emulsion ($W_1/O$) was poured into external aqueous phase ($W_2$), containing PVA and 0.1 % v/v acetic acid under constant stirring. Then, the whole mixture was sonicated under ice bath using ultra probe sonicator for 5 min at 80% sonication amplitude. The resultant double emulsion ($W_1/O/W_2$) was allowed to stirr magnetically at 1000 rpm for 24 hr at room temperature in order to evaporate residual DCM completely and to form CS-PNs. Subsequently, the resulting CS-PNs were centrifuged at 15,000 rpm for 15 min at 4 $^oC$ temperature, using cooling centrifuge (RC 4100 F, Eltek, Mumbai, India). The supernatant was kept for drug content analysis as described later and sediment was washed thrice with doubled distilled water (DDW). CS-PNs were resuspended in DDW containing 2 % (w/v) mannitol as cryoprotectant and finally lyophilized using freeze drier (Labconco, USA) for 48 hr at -45 $^oC$ with a vacuum pressure of 0.050 mbar. The lyophilized CS-PNs were stored in a desiccator at 4 $^oC$ until further use [39].

### 5.1.3 Experimental design

#### 5.1.3.1 Preliminary screening of variables by using Plackett-Burman screening design

A set of experiments with Plackett–Burman statistical experimental design was performed to screen the effect of various formulation and process variables on the critical quality attributes (CQAs) of CS-PNs [177]. The screening phase allows to determine the key variables, which affect significantly on the CQAs, with minimal experimental runs. The Design Expert® software (Version 8.0.6.1, Stat-Ease Inc., Minneapolis, USA) was utilized for the generation of randomized design matrix and evaluation of statistical experimental design. Each variable was represented at two levels, namely, "high" and "low". These levels define the upper and lower limits of the range covered by each variable. The level selection of different variables was based on a preliminary study and findings in the existing scientific literature. Different 11 independent variables were tested at 12 experimental runs. The selected experimental variables along with their levels, used for the screening design are depicted in Table 5.1. The particle size ($Y_1$), % encapsulation efficiency (EE) ($Y_2$) and polydispersity index (PDI) ($Y_3$) were selected as dependent variables (CQAs). Results of the different experimental runs were analyzed by employing multiple linear regressions using one-way analysis of variance (ANOVA), in order to determine the significance of the selected model along with the factor coefficients [178]. Results obtained were statistically analyzed at 5% level of significance. All experiments were performed in a triplicate and randomized order.

**Table 5.1 Experimental variables with their levels in Plackett-Burman screening design**

| Variables | Level | |
|---|---|---|
| Independent Variables | Low (-1) | High (+1) |
| A: Polymer concentration (%w/v) | 0.1 | 0.2 |
| B : Concentration of external surfactant (%w/v) | 0.5 | 1.5 |
| C : Stirring speed (rpm) | 750 | 1250 |
| D : Organic phase/aqueous phase ratio | 0.17 | 0.33 |
| E : Sonication time (min) | 3 | 6 |
| F : Sonication amplitude (%) | 40 | 80 |
| G : Types of organic phase | DCM | CLF |
| H : Concentration of internal surfactant (%w/v) | 0.05 | 0.1 |
| I : Types of drug | CS | GAN |
| J : Ratio of organic phase (DCM/CLF) | 3:2 | 4:1 |
| K : Stirring temp ($^{o}$C) | 25 | 40 |

*Where, DCM: Dichloromethane; CLF: Chloroform; CS: Cromolyn sodium; GAN: Ganciclovir*

### 5.1.3.2 Optimization of variables by using Box-Behnken experimental design

The critical formulation and process variables obtained after preliminary screening through the Plackett-Burman screening design, were applied to response surface methodology (RSM) for statistical optimization of the CS-PNs. The RSM is a powerful statistical technique devoted for designing, modeling and evaluating the influence of variables through statistical model. It also allows to establish the mathematical trend between the dependent and independent variables in the experimental design space with minimum number of experimental runs. In current study, a response surface method (RSM), 3-level, 3-factor, Box-Behnken

experimental design with statistical model incorporating interactive and polynomial terms was utilised for optimization, quantification and establishing the relationship between the clusters of controlled independent variables and the physicochemical properties of CS-PNs, based on selected criteria. The Box-Behnken experimental design consists of a set of different points lying at the midpoint of each edge and the replicated center point of the multidimensional cube [179-181].

Based on initial screening in the preliminary studies, concentration of polymer ($X_1$), concentration of surfactant ($X_2$) and organic phase/aqueous phase ratio ($X_3$) were opted as three critical independent variables. Each critically selected variable is varied at three different levels, which are further coded as +1, 0 and -1 analogous to high, medium and low level, respectively as summarized in Table 5.2. Other variables, which were evaluated in the preliminary Plackett-Burman screening design, were adjusted to the fixed level in the BBD owing to their statistically insignificant effect on the dependent variables. The studied particle size ($Y_1$), EE ($Y_2$) and PDI ($Y_3$) of CS-PNs were used as dependent variables (Table 5.2). The total number of experiments (N) required for the generation of design matrix of Box-Behnken experimental design were decided by considering the following formula (Eq (5.1)):

$$N = 2k (k - 1) + Co \qquad \text{Eq (5.1)}$$

Where, k refers the number of factors and Co is the replicates at center points.

The design matrix comprising of 17 runs, along with quadratic response surface and second order polynomial model was generated by using Design-Expert software® (8.0.6.1, Stat-Ease Inc., Minneapolis, USA). All experiments were performed in a randomized manner to minimize any possible source of experimental errors and thus, to eliminate variability and biasness of the response.

**Table 5.2 Independent variables with their levels and dependent variables in Box-Behnken experimental design**

| Independent variables | Coded levels of variables | | |
|---|---|---|---|
| | **Low** | **Medium** | **High** |
| | -1 | 0 | 1 |
| $X_1$ = Concentration of polymer (%w/v) | 0.1 | 0.15 | 0.2 |
| $X_2$ = Concentration of surfactant (%w/v) | 0.5 | 1 | 1.5 |
| $X_3$ = Organic phase/aqueous phase ratio (v/v) | 0.17 | 0.25 | 0.33 |
| **Dependent variables (Responses)** | **Constraints** | | |
| $Y_1$= Particle size (nm) | Minimize | | |
| $Y_2$= Encapsulation efficiency (%) | Maximize | | |
| $Y_3$= Polydispersity index (PDI) | Minimize | | |

Multiple linear regression was applied by employing the ANOVA, in order to ascertain the influence and significance of factors along with their interactive effect on the response variables as well as adequacy of the developed regression model [181, 182]. The adequacies of the polynomial equations were evaluated by the correlation co-efficient ($R^2$) and determining the lack of fit value. Goodness of fit was judged based on adjusted and predicted $R^2$ values. Similarly, adequate precision (signal to noise ratio) was also derived. Numerical output of ANOVA was represented in terms of *p*-value for evaluating the significance of the model and independent variables on response variables. Results obtained were statistically analyzed at 5% level of significance. Quantitative and qualitative contribution of each independent variable on each of the dependent responses was analyzed. The correlation between two independent variables and response variable as well as design space was ascertained by three dimensional (3D) response surface graphs and two dimensional (2D) contour plots [179, 181].

The statistical influence of independent variables were modeled using following non-linear polynomial equation (Eq (5.2)) generated by the regression analysis in the BBD

$$Y = A_0 + A_1X_1 + A_2X_2 + A_3X_3 + A_4X_1X_2 + A_5X_2X_3 + A_6X_1X_3 + A_7X_1^2 + A_8X_2^2 + A_9X_3^2 + E, \quad \text{Eq (5.2)}$$

in which Y is the measured response of the dependent variable associated with each factor level combination; $A_0$ is an intercept; $A_1$-$A_9$ are the regression coefficients; $A_1$-$A_3$ are the main effect of $X_1$-$X_3$; $A_4$-$A_6$ are the interactive effect of the main factors; $A_7$-$A_9$ are the quadratic effects of the independent variables, and E is the random error term [45].

After generating the polynomial equations for the respective dependent variables, CS-PNs were optimized by employing numerical optimization technique to find out the levels of independent variables that would yield CS-PNs with desired quality traits. The constraints for dependent variables were fixed in order to obtain CS-PNs with maximum EE and minimum particle size with low PDI. Desirability function was probed for combining all the responses in one measurement in order to predict the optimum levels for the independent variables. By considering this fact, the optimization was performed through the software for obtaining the best preferable formulation. Subsequently, the experimentally optimized formulation was prepared and tested to verify the correlation between the actual and predicted responses and thereby, validity of the model [23, 45, 179, 183]. The optimized CS-PNs were further subjected to various characterizations, *in-vitro* and *in-vivo* evaluation studies.

### 5.1.4 Characterizations of CS-PNs

#### 5.1.4.1 Particle size, polydispersity index (PDI) and zeta potential

Measurement of particle size, zeta potential and PDI of prepared CS-PNs was carried out by photon correlation spectroscopy using DELSA$^{TM}$ NANO C particle size analyzer (Beckman Coulter, Inc., UK) at 25 $^{o}$C temperature. CS-PNs were diluted properly (1:10) with DDW to derive the optimum kilo counts per second (Kcps) of 50 to 200 and kept in polystyrene cuvettes for the measurement. All measurements were conducted using He-Ne laser generated scattering light at a fixed scattering angle of 165° and rate of fluctuations in intensity of laser light due to scattering of suspended particles during their Brownian motion were determined. The distribution of particle size of nanoparticles is reported as a PDI. It is dimensionless entity ranging from 0 to 1, which reveals the nature of distribution such as monodispersed or polydispersed. The values close to 0 indicates the monodispered nature of the dispersion [184, 185].

The electrophoretic mobility of charged CS-PNs, under the influence of an applied electric field was measured for determination of zeta potential. Samples were prepared by using the same protocol as above at 25 $^{o}$C temperature. Diluted dispersion of CS-PNs was placed in the photoelectric cell under the electric field for the measurement of surface electric charge based on Helmholtz-Smoluchowski equation [185, 186]. All measurements were performed in the triplicates and mean value considered for the analysis of data.

#### 5.1.4.2. Encapsulation efficiency (EE) and drug loading

The EE (%) and drug loading (%) of prepared CS-PNs was determined indirectly by calculating the amount of free CS (un-entrapped) in the aqueous phase of the dispersion of CS-PNs as reported previously [23, 29, 45]. Briefly, prepared CS-PNs

dispersion was centrifuged at 15,000 rpm for 15 minutes at 4 $^{o}$C using cooling centrifuge in order to separate the nanoparticles from the unentrapped drug containing aqueous phase. The clear supernatant obtained after centrifugation was decanted, appropriately diluted and analyzed for free CS content by spectrophotometrically (Shimadzu UV 1800, Japan) at $\lambda_{max}$ of 239 nm. The EE (%) and drug loading (%) of CS-PNs were calculated according to the following formula (Eq (5.3) & Eq (5.4)):

$$EE\ (\%) = \frac{Total\ amount\ of\ CS\ added - Amount\ of\ free\ CS\ in\ supernatant}{Total\ amount\ of\ CS\ added} \times 100$$

Eq (5.3)

$$Drug\ loading\ (\%) = \frac{Amount\ of\ CS\ loaded\ into\ nanoparticles}{Total\ amount\ of\ prepared\ nanoparticles} \times 100$$

Eq (5.4)

### 5.1.4.3 Solid state characterizations

#### 5.1.4.3.1 Fourier transform infrared spectroscopy (FTIR) study

The FTIR spectra of pure CS, PLGA, PVA and optimized CS-PNs were recorded by following the same protocol and same instrument as mentioned in the ***sub-section 5.1.1.2.1*** in order to evaluate any significant change, if occurs, during the encapsulation of CS inside the nanoparticles. The scanning was performed over the wavenumber ranging from 4000 to 400 $cm^{-1}$ at room temperature and the resolution was set at 4 $cm^{-1}$.

#### 5.1.4.3.2 Differential scanning calorimetry (DSC) study

The physical state of CS inside nanoparticles was assessed by DSC study. The thermograms of pure CS, PLGA, PVA and optimized CS-PNs were recorded by

following the same protocol and same instrument as mentioned in the ***sub-section 5.1.1.2.2***.

#### 5.1.4.3.3 Powder X-ray diffractometry (PXRD) study

The crystallographic structure of CS as well as change in the physical state of CS during the encapsulation process was studied by PXRD. The PXRD patterns of pure CS, PLGA, PVA, physical mixture and optimized CS-PNs were obtained on Rigaku portable X-ray diffractometer (Rigaku, Japan) equipped with 2θ compensating slit. The X-ray radiation source was monochromatic Cu $K\alpha_1$ radiation ($\lambda$=1.54187 Å), generated at a voltage of 40 kV and 25 mA current by passing through nickel filter. The diffraction patterns were collected at room temperature, by mounting the samples on zero-background sample holder and recorded over the 2θ scanning range from 5° to 50° with a step size 0.01° at 2 °/min scanning speed, with step time of 0.5 sec [23, 39, 49].

### 5.1.4.4 Shape and surface morphology

#### 5.1.4.4.1 High resolution transmission electron microscopy (HR-TEM)

The shape and surface morphology of the optimized CS-PNs was examined by employing HR-TEM. Briefly, a drop of appropriately diluted CS-PNs was placed on the carbon-coated copper grid and negatively stained with 2 %w/v phosphotungastic acid. The excess of dispersion was wicked off with filter paper and grid was allowed to air dry at room temperature. Then, the grid was examined using TEM (TECHNAI-$20G^2$, FEI, Philips, Holland) operated at an accelerating voltage of 200 keV having magnification of 0.23 nm. Digital images were visualized at different magnifications and captured with CCD camera [39, 45].

#### 5.1.4.4.2 Atomic force microscopy (AFM)

The surface morphology of optimized CS-PNs was visualized by atomic force microscope (NT-MDT, Moscow, Russia). Briefly, a drop of diluted CS-PNs was deposited on freshly cleaved mica and allowed to immobilize for 1-2 min, subsequently air dried at room temperature to form thin film. Then, surface morphology of CS-PNs was visualized by mounting on AFM scanner and imaged in semicontact mode with scanning rate of 0.5 Hz. Image acquisitions and dimensional analysis was performed using SOLVER NEXT software [23, 188].

### 5.1.4.5 *In-vitro* drug release study

The *in-vitro* drug release study of optimized CS-PNs was performed using modified dialysis bag diffusion technique in phosphate buffer pH 7.4 [23, 45, 189]. The dialysis membrane (molecular weight cut-off 12-14 kDa) has capability to retain the nanoparticles, but allows the transfer of the dissolved or released drug molecules in to the release media [190]. In brief, 3 ml of optimized CS-PNs dispersion (3 ml equivalent to 10 mg of CS) was placed in a pre-soaked dialysis bag. After that, both ends of dialysis bag were tightly fastened and immersed in 150 ml of phosphate buffer pH 7.4 containing flask, maintained at 37 ± 0.5 $^{o}$C under continuous stirring at 100 rpm speed on magnetic stirrer. The receptor compartment was covered to prevent the evaporation of dissolution medium. An aliquot of 5 ml of dialysate sample was withdrawn at regular time intervals and were replaced with an equal volume of fresh pre-warmed media in order to maintain sink condition throughout experimentation. Withdrawn samples were filtered through 0.2 µ syringe filters and suitability diluted for analyzing drug content spectrophotometrically at $\lambda_{max}$ of 239 nm. *In-vitro* drug release data were further fitted to various release kinetic models, including zero-order

model, first-order model, Higuchi model and Korsemeyer-Peppas model, in order to ascertain the release kinetics and mechanism of drug release involved from the nanoparticles. The correlation coefficient ($R^2$) was determined by regression analysis to determine the linearization and goodness of fitting of kinetic model. Each experiment was run in triplicate. Release kinetic modeling was performed by employing following set of equations.

Zero order : $Q_t = Q_0 + Kt$ Eq (5.5)

First order : $Q_t = Q_0 e^{-Kt}$ or $\log Q_t = \log Q_0 + Kt/2.303$ Eq (5.6)

Higuchi model : $Q_t/Q_0 = Kt^{½}$ Eq (5.7)

Korsmeyer–Peppas : $Q_t/Q_0 = Kt^n$ Eq (5.8)

Where, $Q_0$ is the initial amount of drug in the release media, $Q_t$ is the amount of released drug at time 't' present in the release media, K is the release kinetic rate constant, t is time, $Q_t/Q_0$ is the fraction of drug released after time 't' and n is release exponent, which characterizes the drug release mechanism. The value of $n \leq 0.5$ indicates Fickian diffusion (Case I), $0.5 < n < 1$ indicates non-Fickian release (anomalous transport), $n=1$ indicates case-II transport (zero-order release) and $n < 1.0$ indicates super case-II transport [191, 192].

**5.1.4.6 Accelerated and real time storage stability study**

The stability of CS-PNs was assessed over a period of 6 month at room temperature (25 $\pm$ 2 $^{o}$C), refrigerated condition (4 $\pm$ 1 $^{o}$C), and accelerated condition (40 $\pm$ 2 $^{o}$C/75 $\pm$ 5 % RH) as per International Conference on Harmonization (ICH) Q1A (R2) guidelines and previously reported method. Lyophilized CS-PNs were sealed in glass vials and placed in stability chamber (Narang Industries, Mumbai, India) at different environmental conditions for the total period of 6 months. Samples were

withdrawn at different time intervals (0, 1, 2, 3 and 6 months) and analyzed for any change in the physicochemical attributes in terms of physical appearance, particle size, PDI and EE according to the above mentioned protocols [45, 193].

#### 5.1.4.7 Animal studies

##### 5.1.4.7.1 Animals

The animal study protocol was duly approved by Central Animal Ethical Committee of Banaras Hindu University (No. Dean/2014/CAEC/856). All the animal studies were carried out in accordance with the guidelines of CPCSEA (Committee for the Purpose of Control and Supervision of Experiments on Animal), Ministry of Social Justice and Empowerment, Government of India, New Delhi. Adult Charles Foster (CF) rats (225 ± 20 g) of either sex were used for all the animal studies. Animals were housed in propylene cages under standard laboratory conditions with a 12 hr light/dark cycle for one week before the experiment. They had free access to standard rodent diet with water *ad libitum.* Animals were fasted overnight prior to 12 hr of experiment but had free access to water. Animals were sacrificed by euthanasia, and disposal of the used animals was done by burning them using an incinerator. All efforts were made in order to reduce animal suffering [23].

##### 5.1.4.7.2 *Ex-vivo* intestinal permeation study

The intestinal permeation potential of CS-PNs across the GIT was assessed by *ex-vivo* intestinal permeation study using non-everted gut sac technique, which simulates *in-vivo* permeation conditions [107]. Healthy rats of either sex were divided into two groups (n=3) and sacrificed by cervical dislocation under excessive ether anesthesia. The small intestine was isolated by abdominal incision and immediately placed into ice-cold, bubbled (carbogen, 95:5 $O_2/CO_2$) saline solution [45]. The small intestine,

20-30 cm distal from the pyloric sphincter was flushed with physiological saline solution using a blunt end syringe, to remove any intestinal content and cut into segments. The CS solution (1 ml equivalent to 10 mg/ml) and CS-PNs (1 ml equivalent to 10 mg/ml) were filled in intestinal sac using syringe and tied on both sides with a thread. Each filled intestinal sac was mounted in 40 ml phosphate buffer pH 7.4 filled conical flasks, maintained at 37 $\pm$ 0.5 $^{o}$C with continuous aeration (carbogen, 95:5 $O_2/CO_2$) using laboratory aerator. At predetermined time intervals, samples were withdrawn from receptor compartment (conical flask) and replenished with an equal volume of fresh, pre-warmed buffer solution. Withdrawn samples were sonicated (for 15 min), filtered through 0.2 µ membrane syringe filters and suitability diluted in order to analyze for CS content spectrophotometrically at $\lambda_{max}$ of 239 nm [23, 194, 195]. Apparent permeability coefficients (Papp) for CS as well as CS-PNs were calculated using following formula (Eq (5.9)) and expressed in cm/s.

$$P\text{app} = \frac{\partial Q}{\partial t} \times \frac{1}{ACo} \qquad \text{Eq (5.9)}$$

Where $\partial Q/\partial t$ is the steady-state appearance rate of CS-PNs/CS in the receiver compartment, A is the exposed intestinal tissue surface area ($cm^2$) and $C_o$ is the initial concentration of the CS in the donor compartment at zero time.

Permeability enhancement ratio for CS was calculated according to following formula (Eq (5.10)).

$$\text{Permeability enhancement ratio} = \frac{\text{Papp of CS encapsulated polymeric nanoparticless}}{\text{Papp of CS solution}}$$

Eq (5.10)

#### 5.1.4.7.3 *In-vivo* intestinal uptake study

The intestinal particulate uptake and thereby, permeation of CS-PNs was visualized by *in-vivo* intestinal uptake study using confocal laser scanning microscopy (CLSM) upon oral administration in rats. FITC tagged CS-PNs were administered orally (20 mg/kg) with the aid of oral gavage to overnight fasted rats. After 2 hr of oral administration, rats were sacrificed by euthanasia. Small intestine was removed by abdominal incision, washed with physiological saline solution and preserved with 10 % neutral buffered formalin solution till cryosectioning. Tissue samples were washed with phosphate buffer solution. Cryoblocks were prepared by embedding tissue samples in cryostat media (OCT) and freezing with liquid nitrogen. The blocks were further freezed in deep freezer (SANYO VP, India) at -82 $^{o}$C for 30 min. The intestinal transverse-sections of 5 μm thickness were sliced, using the cryo-microtome (Leica CM1850, Leica Microsystem srl, Milan, Italy) at -20 $^{o}$C. The sections were placed on poly-l-lysine coated slides and stored at 37 $^{o}$C temperature for 20 min for the fixation of section. The coverslip was mounted on the section by adding 15 μl of Vectashield® (Vector laboratories, Inc., USA) mounting medium in dark to prevent the reduction of fluorescence. The uptake and permeation of CS-PNs in the intestinal mucosa was observed by visualizing the transverse-section as well as apical view of intestine, under a LSM 510 META confocal microscope (Carl Zeiss Inc., USA) at different magnification with excitation wavelength of 488 nm [67, 106, 196, 197].

#### 5.1.4.7.4 *In-vivo* pharmacokinetic study

##### 5.1.4.7.4.1 *Dosing and sampling*

*In-vivo* pharmacokinetic study was performed by the previously reported methods [23, 106, 107, 198]. Over-night fasted rats were randomly divided into three groups

(n=6 rats per each group) for single dose oral bioavailability study. Each group received formulations orally at a dose of 20 mg/kg body weight of animal with dose volume of 500 µl, for maintaining the dose constant. Group I received CS solution whereas Group II was administered with CS-PNs for relative pharmacokinetic profiling. Group III served as control, which received only saline solution. Following the oral administration, serial blood samples (250 µl) were withdrawn from retro-orbital venous plexus at different pre-specified time intervals (0.5, 1, 1.5, 2, 4, 8, 12 and 24 hr), under mild ether anesthesia and collected into heparinized micro-centrifuge tubes. The blood loss was compensated by injecting equivalent volume of normal saline solution followed by blood sampling. Plasma was separated after blood collection by centrifugation at 5000 rpm for 5 min at -4 $^{o}$C and frozen at -20 $^{o}$C till further analysis.

#### 5.1.4.7.4.2 *Chromatography conditions and drug extraction*

CS concentration in plasma samples was measured by the earlier reported and in-house validated RP-HPLC (Shimadzu Corporation, Koyoto, Japan) method as described in ***sub-section 4.1.2***. The details of chromatography conditions and drug extraction are mentioned in ***sub-section 4.1.2.1 and 4.1.2.4***, respectively.

#### 5.1.4.7.4.3 *Pharmacokinetic parameters*

Various pharmacokinetic parameters were determined for CS solution and CS-PNs using non-compartmental analysis of plasma drug concentration-time profile data through Winnonlin® 6.1 (Pharsight Corporation, Mountain View, CA) pharmacokinetic software. All pharmacokinetics parameters including Peak plasma concentration ($C_{max}$), time to achieve peak plasma concentration ($T_{max}$), half-life ($T_{1/2}$) and mean residence time (MRT) were estimated. The area under the concentration–

time curve ($AUC_{0\text{-}24h}$) was calculated using the trapezoidal method and was further extrapolated to infinity ($AUC_{0\text{-}\infty}$).

**5.1.4.7.5 *In-vivo* mast cell stabilizing activity**

*In-vivo* mast cell stabilizing activity was studied by following the protocol as reported by Gupta *et al*. [199]. Healthy rats were randomly divided into four groups (n=6 rats per group) for studying mast cell stabilizing activity. Group I and II were kept as normal control and positive control, respectively, which received only saline solution orally. Group III and IV were orally administered with CS solution and CS-PNs, respectively, at a dose of 20 mg/kg with dose volume of 500 µl, for continuous 7 days prior to collection of mast cells. On $7^{th}$ day, after 2 hr of administration of respective formulations, rats were anesthetized and injected with 5 ml of pre-warmed (37°C) Tyrode buffer B solution (137 mM NaCl; 2.7 mM KCl; 1 mM $MgCl_2$; 0.5 mM $CaCl_2$; 0.4 mM $NaH_2PO_4$; 5.6 mM Glucose; 10 mM HEPES; pH ~7.4) into the peritoneal cavity. The abdomen was massaged gently for 90 s. A midline incision was made and the peritoneum was exposed. The pale fluid was aspirated using a blunted plastic Pasteur pipette and collected in a plastic centrifuge tube containing 7-10 ml of RPMI 1640 (pH 7.2-7.4) with 2 ml of metrizamide. The cells remaining at the buffer metrizamide interface were aspirated and discarded. The fluid was then centrifuged at 1000 rpm for 10 min at room temperature and the supernatant discarded to reveal a cell pellet. The cell pellets were re-suspended in fresh Tyrode buffer B. Aliquots of the cell suspension were incubated (except normal control) with the 0.1 ml of 2 µg/ml mast cell activator compound 48/80 for 15 min at 37 $^{o}$C. The aliquots were carefully spread over glass slides and the mast cells were stained with 1% toluidine blue. The slides were dried in air and the mast cells counted from randomly selected high power objective fields (45X) for the determination of percentage protection against mast cell

degranulation [200-202]. Remaining aliquots were centrifuged and supernatant was analyzed for histamine release by o-phthaldialdehyde spectrofluorometric method [203].

#### 5.1.4.8 Statistical analysis

All the experiments were performed in triplicate and results were presented as mean ± standard deviation (SD), except *in-vivo* study, in which results were expressed as mean ± standard error of mean (SEM). GraphPad Prism software (version 5.03, GraphPad Software, USA) was used for statistical comparisons of the results to control. Statistical analysis of the results were performed using student (unpaired) t-test and one-way ANOVA test. The differences were assumed statistical significant when $p<0.05$ (95% confidence interval).

## 5.2 Results and discussions

### 5.2.1 Pre-formulation studies

#### 5.2.1.1 Solubility study

CS exhibited pH dependent solubility at 25 ± 2 $^{o}$C and the results are shown in Figure 5.1. The higher solubility of CS was exhibited in water, phosphate buffer pH 6.8 and phosphate buffer pH 7.4. The lowest solubility was found in acidic buffer pH 1.2. The solubility of pure CS was found to be 0.145 ± 0.007, 76.321 ± 3.864, 90.121 ± 4.51 and 98.245 ± 1.284 mg/ml in acidic buffer pH 1.2, phosphate buffer pH 6.8, water and phosphate buffer pH 7.4, respectively.

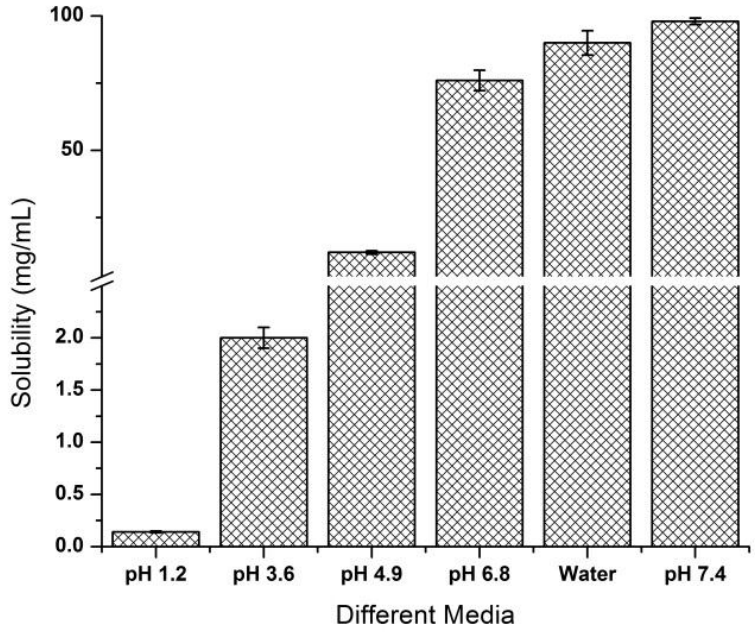


**Figure 5.1 Solubility profile of CS in different media at 25 ± 2 °C (vertical bars represent ±SD; n=3)**

In the formulation of nanoparticles, encapsulation of hydrophobic drugs has not been affected by the employed aqueous phase, owing to their very low aqueous solubility. In case of hydrophilic drugs, the poor encapsulation in nanoparticles was observed with the use of normal aqueous phase. The drug being soluble in the aqueous phase is not available for encapsulation into the polymer/lipid carrier during preparation of nanoparticles and this leads to poor encapsulation in nanoparticles. To overcome this problem, the aqueous phase having limited capability to solubilize the drug should be selected, which will reduce the solubility and subsequently, improves the availability of drug to get encapsulated into the nanoparticles [176]. Hence, based on results and existing scientific literature, we used acidic aqueous phase as external phase for the preparation of nanoparticles [45, 204].

### 5.2.1.2 Drug excipients compatibility studies

#### 5.2.1.2.1 Fourier transform infrared (FTIR) spectroscopy

FTIR study was performed in order to evaluate the interaction, if occurs as well as to confirm the compatibility between CS and excipients. The FTIR spectra of PLGA, CS, PVA and their physical mixture are shown in Figure 5.2. As depicted in (Figure 5.2 (a)), FTIR spectra of CS showed the basic peaks at 1639.54 $cm^{-1}$ and 3416 $cm^{-1}$, assigned to the C=O and O-H stretching as well as characteristic peaks at 2880 $cm^{-1}$ (C-H alkane), 1477 $cm^{-1}$ (aromatic C-H), 1573 $cm^{-1}$ and 1410 $cm^{-1}$ (asymmetric and symmetric $COO^{-}$). Moreover, the vibrations within a molecule were noticed through the large number of characteristic bands in fingerprint region (1400–600 $cm^{-1}$) [43, 45].

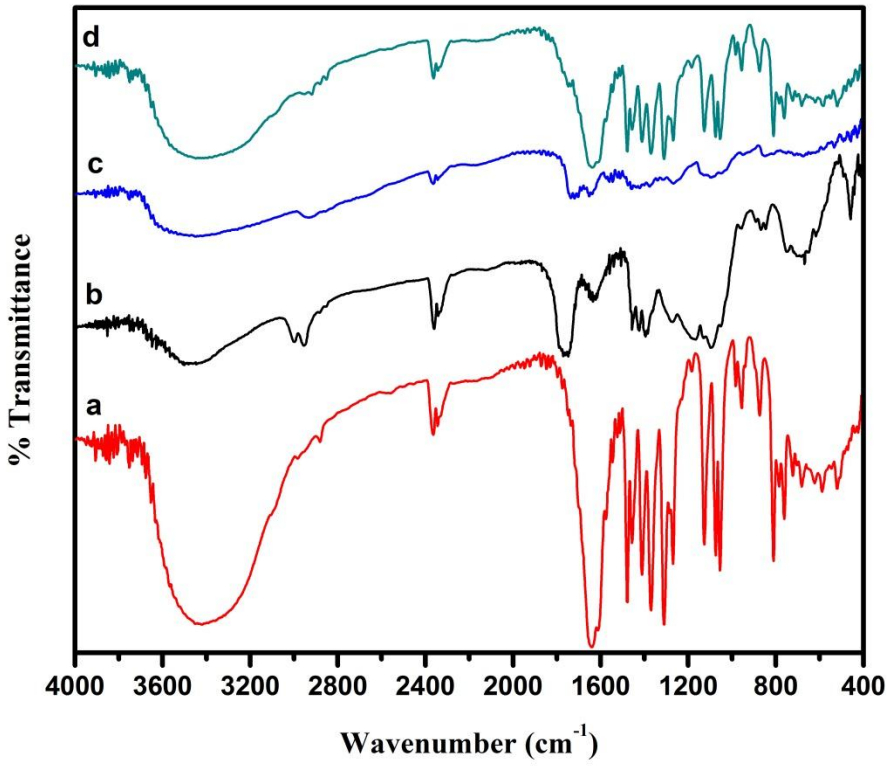


**Figure 5.2 FTIR spectra of (a) CS, (b) PLGA, (c) PVA and (d) physical mixture**

FTIR spectra of PLGA (Figure 5.2 (b)) showed various bands at 1748.12 $cm^{-1}$ (C=O stretching), 1194.25 $cm^{-1}$ (C-O stretching), 2948.47 $cm^{-1}$ (C-H stretching) and broad bands between 3200-3600 $cm^{-1}$ owing to its terminal hydroxyl group [205]. FTIR spectrum of PVA (Figure 5.2 (c)) exhibited various peaks in the range of 2840-3000 $cm^{-1}$ (C-H stretching), 3200-3550 $cm^{-1}$ (O-H stretching) and 1750-1735 $cm^{-1}$ (C=O and C-O stretching from acetate group) [206]. The FTIR spectra of the physical mixture (Figure 5.2 (d)) showed all the major peaks corresponding to CS, PLGA and PVA at nearly same wavenumber, suggesting the absence of interaction of CS with other excipients and existence of compatibility with each other [40].

**5.2.1.2.2 Differential scanning calorimetry (DSC) study**

DSC thermograms of CS, PLGA, PVA and their physical mixture are depicted in Figure 5.3. The pure CS showed sharp endothermic peak at 264 $^{o}$C corresponding to its melting point, suggesting the crystalline nature of drug (Figure 5.3 (a)) [45, 149]. PLGA and PVA exhibited sharp endothermic peak at 65 $^{o}$C and 226 $^{o}$C, respectively (Figure 5.3 (b) & (c)). CS maintained its crystalline characteristic in the physical mixture without any considerable shift in endothermic peak, confirming the absence of interaction of CS with excipients [39, 45, 207]. Moreover, no any new endothermic or degradation peak was observed in the thermogram of physical mixture, suggesting the existence of compatibility between CS and other excipients (Figure 5.3 (d)).

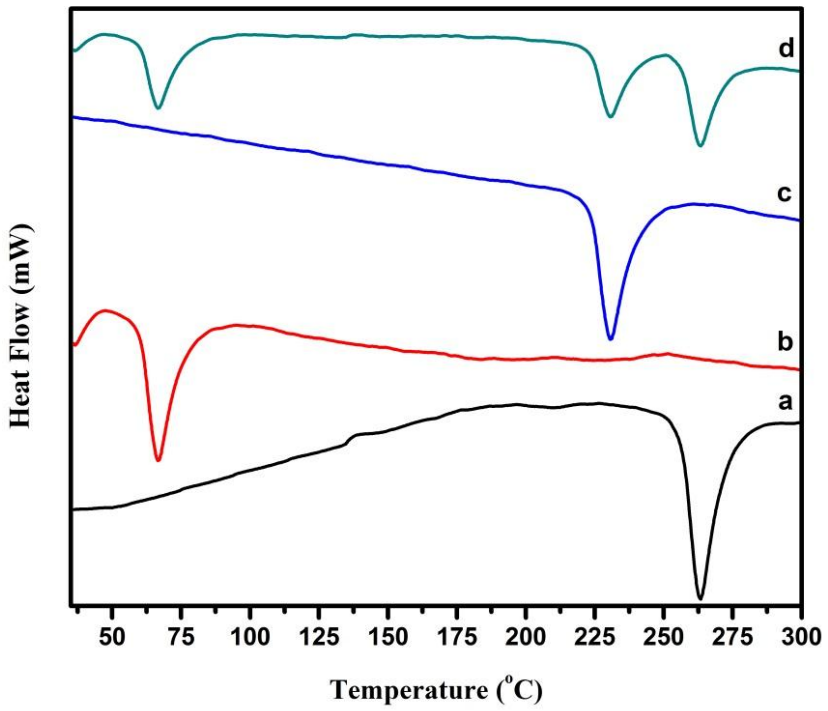


**Figure 5.3 DSC thermograms of (a) CS, (b) PLGA, (c) PVA and (d) physical mixture.**

### 5.2.2 Experimental design

#### 5.2.2.1 Preliminary screening of variables by using Plackett-Burman screening design

The physicochemical properties of CS-PNs prepared by double emulsification solvent evaporation ($W_1/O/W_2$) method are influenced by various formulation and process variables. The influence of various independent variables on the particle size, EE and PDI of the CS-PNs (CQAs) were studied by 11-factor, 2-level Plackett-Burman screening design. The Plackett-Burman statistical experimental design was employed for the initial screening and selection of critical variables affecting significantly to the formulation characteristics of CS-PNs, with good degree of accuracy during preliminary studies. It is a useful and efficient mathematical approach for evaluating

the effect of large number of independent variables on particular CQAs by performing relatively few numbers of experimental runs [208, 209]. A total of 12 experimental trials, comprising of various combinations of different 11 independent variables were carried out as shown in Table 5.3. Since Plackett-Burman screening designs are resolution 4 designs, only main effects of the selected independent variables were analyzed. The wide variation was observed in the selected dependent variables of CS-PNs, suggesting that the independent variables had a significant effect on the response parameters chosen. Table 5.4 shows the results of different experimental runs in terms of different dependent variables. Pareto chart showing the relative effect of the each independent variable on each dependent variable is depicted in Figure 5.4. It indicates the effect of independent variables plotted against the vertical axis as per their respective rank order. The variables for which vertical bars extending passed the horizontal line suggested the statistical significance on the dependent variable [210].

**Table 5.3 Plackett-Burman screening design experimental matrix**

| Run | A | B | C | D | E | F | G | H | I | J | K |
|---|---|---|---|---|---|---|---|---|---|---|---|
| 1 | 0.20 | 1.50 | 1250 | 0.17 | 3 | 40 | CLF | 0.05 | GAN | 4:1 | 25 |
| 2 | 0.10 | 1.50 | 1250 | 0.17 | 6 | 80 | CLF | 0.05 | CS | 3:2 | 40 |
| 3 | 0.10 | 1.50 | 1250 | 0.33 | 3 | 40 | DCM | 0.1 | CS | 4:1 | 40 |
| 4 | 0.10 | 0.50 | 1250 | 0.17 | 6 | 80 | DCM | 0.1 | GAN | 4:1 | 25 |
| 5 | 0.10 | 1.50 | 750 | 0.33 | 6 | 40 | CLF | 0.1 | GAN | 3:2 | 25 |
| 6 | 0.20 | 1.50 | 750 | 0.17 | 3 | 80 | DCM | 0.1 | GAN | 3:2 | 40 |
| 7 | 0.20 | 0.50 | 750 | 0.17 | 6 | 40 | CLF | 0.1 | CS | 4:1 | 40 |
| 8 | 0.20 | 1.50 | 750 | 0.33 | 6 | 80 | DCM | 0.05 | CS | 4:1 | 25 |
| 9 | 0.10 | 0.50 | 750 | 0.33 | 3 | 80 | CLF | 0.05 | GAN | 4:1 | 40 |
| 10 | 0.10 | 0.50 | 750 | 0.17 | 3 | 40 | DCM | 0.05 | CS | 3:2 | 25 |
| 11 | 0.20 | 0.50 | 1250 | 0.33 | 6 | 40 | DCM | 0.05 | GAN | 3:2 | 40 |
| 12 | 0.20 | 0.50 | 1250 | 0.33 | 3 | 80 | CLF | 0.05 | CS | 3:2 | 25 |

*Where, DCM: Dichloromethane; CLF: Chloroform; CS: Cromolyn sodium; GAN: Ganciclovir*

**Table 5.4 Results of dependent variables obtained through Plackett-Burman design.**

| Run | Particle Size (nm) | EE (%) | PDI |
|---|---|---|---|
| 1 | 396.1 ± 4.3 | 36.8 ± 0.3 | 0.411 ± 0.012 |
| 2 | 290.5 ± 1.2 | 22.8 ± 0.1 | 0.241 ± 0.038 |
| 3 | 230.3 ± 2.4 | 19.3 ± 1.2 | 0.175 ± 0.039 |
| 4 | 382.5 ± 0.7 | 35.1 ± 0.6 | 0.364 ± 0.078 |
| 5 | 215.1 ± 5.1 | 15.7 ± 1.8 | 0.151 ± 0.045 |
| 6 | 387.3 ± 2.8 | 34.4 ± 1.3 | 0.387 ± 0.019 |
| 7 | 398 ± 6.1 | 37.2 ± 0.4 | 0.418 ± 0.084 |
| 8 | 315.2 ± 3.6 | 27 ± 0.7 | 0.287 ± 0.063 |
| 9 | 294.8 ± 0.4 | 23.6 ± 1.6 | 0.254 ± 0.042 |
| 10 | 368.9 ± 8.4 | 36.5 ± 0.6 | 0.341 ± 0.031 |
| 11 | 392.5 ± 3.8 | 36.2 ± 0.2 | 0.398 ± 0.094 |
| 12 | 376 ± 3.2 | 34.2 ± 0.7 | 0.352 ± 0.059 |

*All values reported are mean±SD; n = 3*

Statistical analysis revealed that the particle size ($Y_1$) of the CS-PNs was significantly ($p$<0.05) influenced by three independent variables, i.e., concentration of polymer (A), concentration of surfactant (B) and organic phase/aqueous phase ratio (D), as indicated in Figure 5.4 (A) and Table 5.5. The value of correlation coefficient ($R^2$) was found to be 0.9292, indicating the goodness of fit of the model being tested. The $p$-value for the regression model was found to be <0.0001 and was considered as significant. All other independent variables showed non-significant ($p$>0.05) impact on the particle size. The model fitting values for different dependent variables, which indicate model adequacy are listed in Table 5.6.

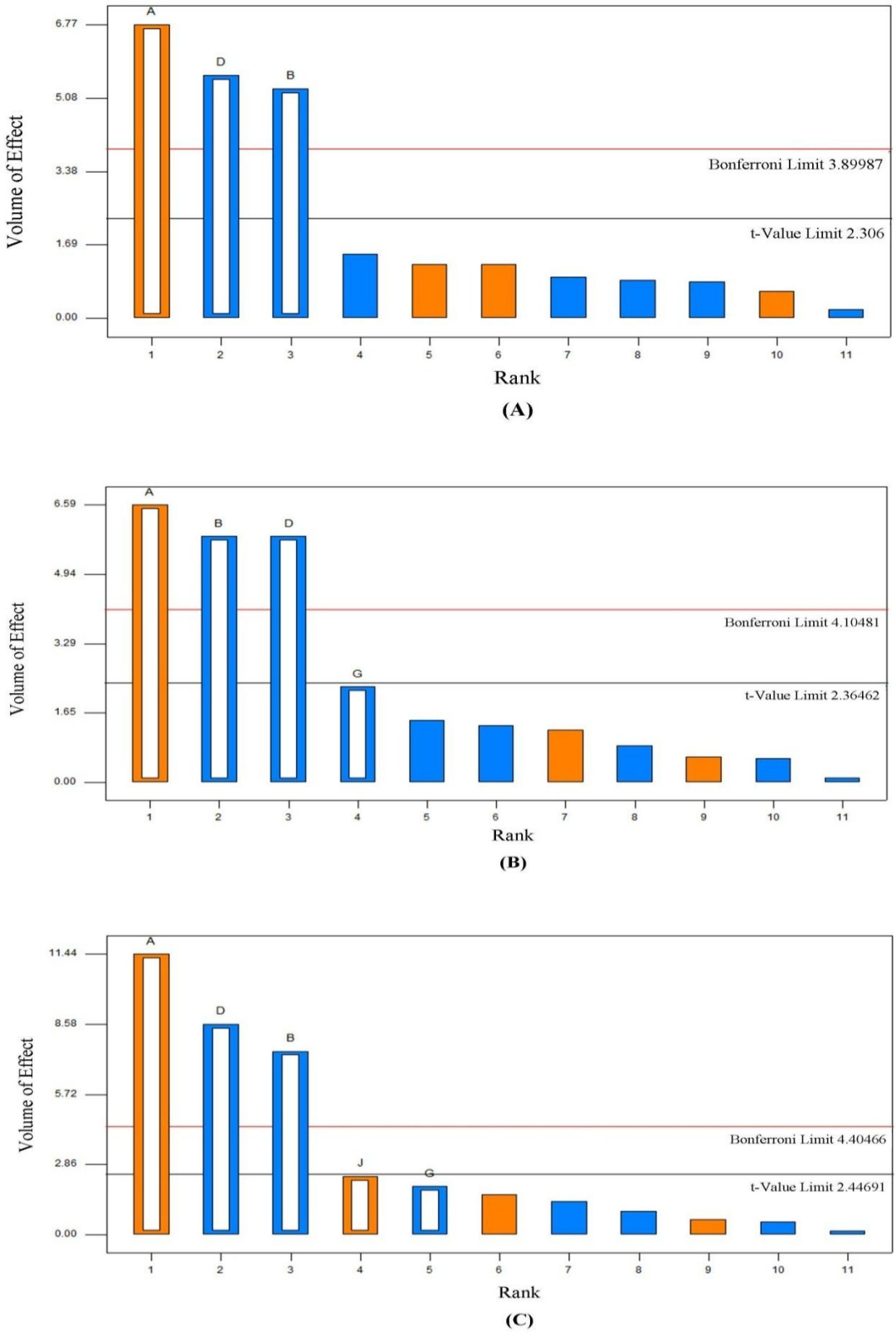


**Figure 5.4 Pareto charts showing the significant effect of independent variables on (A) particle size, (B) EE and (C) PDI of CS-PNs during Plackett-Burman screening design**

**Table 5.5 Statistical analysis of dependent variables of Plackett-Burman screening design**

| Factor | $Y_1$ = Particle size | | $Y_2$ = EE | | $Y_3$ = PDI | |
|---|---|---|---|---|---|---|
| | **Coefficient** | ***p* Value** | **Coefficient** | ***p* Value** | **Coefficient** | ***p* Value** |
| A | 40.33 | 0.0001 | 4.40 | 0.0003 | 0.061 | <0.0001 |
| B | -31.50 | 0.0007 | -3.90 | 0.0006 | -0.040 | 0.0003 |
| C | 7.33 | 0.1959 | 0.83 | 0.1079 | 0.0085 | 0.1056 |
| D | -33.33 | 0.0005 | -3.90 | 0.0006 | -0.045 | 0.0001 |
| E | -5 | 0.2075 | -0.90 | 0.1433 | -0.0050 | 0.1345 |
| F | 3.67 | 0.1961 | -0.38 | 0.1096 | -0.0075 | 0.1000 |
| G | -8.83 | 0.1476 | -1.52 | 0.0574 | -0.010 | 0.0968 |
| H | -11.33 | 0.2369 | -1.17 | 0.1679 | -0.014 | 0.1010 |
| I | 7.33 | 0.1596 | 0.40 | 0.2832 | 0.013 | 0.0551 |
| J | -1.17 | 0.1000 | -0.067 | 0.1000 | 0.0032 | 0.2482 |
| K | -5.17 | 0.2511 | -0.98 | 0.1520 | -0.0027 | 0.1695 |

For EE ($Y_2$) of the CS-PNs, the three most significant ($p<0.05$) independent variables were concentration of polymer (A), concentration of surfactant (B) and organic phase/aqueous phase ratio (D) amongst all other independent variables selected, as depicted in Figure 5.4 (B) and Table 5.5. The $R^2$ value for the regression model was 0.9434, indicating the goodness of fit of the model being tested. The *p*-value for the regression model was found to be significant ($p=0.0002$), confirming the adequate fitting to the model. All other independent variables also affected EE but their impact was statistically non-significant ($p>0.05$).

**Table 5.6 Model summary statistics of the quadratic response surface models**

| Response Variable | Model | | | | | | |
|---|---|---|---|---|---|---|---|
| | **F-value** | **Prob>F*** | **$R^2$** | **Adj. $R^2$** | **Pred. $R^2$** | **Adeq. Prec.** | **C.V. (%)** |
| $Y_1$ | 35.00 | <0.0001 | 0.9292 | 0.9027 | 0.8407 | 17.645 | 6.13 |
| $Y_2$ | 29.18 | 0.0002 | 0.9434 | 0.9111 | 0.8337 | 16.337 | 7.74 |
| $Y_3$ | 53.93 | <0.0001 | 0.9782 | 0.9601 | 0.9129 | 20.833 | 5.83 |

*Adj. $R^2$: Adjusted $R^2$; Pred. $R^2$: Predicted $R^2$; Adeq. Prec.: Adequate Precision; C.V.: Coefficient of Variation; *Prob>F is the significance level and a value less than 0.05 considered significant.*

Similar to particle size, PDI of the CS-PNs was found to be most significantly ($p$<0.05) dependent on the concentration of polymer (A), concentration of surfactant (B) and organic phase/aqueous phase ratio (D) relative to other variables, as observed in Figure 5.4 (C) and Table 5.5. The $R^2$ value for the regression model was found to be 0.9782, suggesting the significant goodness of fit of the model. The significant $p$-value ($p$<0.0001) for the regression model confirmed the adequate fitting to the model. All other independent variables showed non-significant ($p$>0.05) impact on the PDI. Thus, on the basis of results of the Plackett-Burman screening design, all the significantly affected independent variables on the physicochemical properties of CS-PNs were further evaluated by RSM for statistical optimization [209, 210].

#### 5.2.2.2 Formulation optimization of variables by using Box-Behnken experimental design

According to the results obtained from the Plackett-Burman screening design, the total of three independent variables, namely concentration of polymer, concentration of surfactant and organic phase/aqueous phase ratio were selected as critical variables for the statistical optimization of the CS-PNs using RSM [39, 210]. A 3-level, 3-factor

Box-Behnken experimental design based RSM was performed for precisely exploring and optimizing the influence of three independent variables i.e. concentration of polymer ($X_1$), concentration of surfactant ($X_2$) and organic phase/aqueous phase ratio ($X_3$) on dependent variables such as particle size ($Y_1$), EE ($Y_2$) and PDI ($Y_3$) of CS-PNs. A total of 17 batches of CS-PNs including 5 center points, were prepared as per design matrix generated by Box-Behnken experimental design by varying the three independent variables for all possible combinations. All the other independent variables used in the Plackett-Burman screening design, were found to have statistically non-significant effect on the physicochemical properties of CS-PNs in the selected range and hence, set to fix level during optimization using RSM [210]. The statistical treatment combinations of the different independent variables along with the measured response variables obtained by performing experiments are summarized in Table 5.7.

Regression models and polynomial equations explaining the main effect, interactive effect as well as quadratic effect of the various independent variables on dependent variables were generated by fitting the results of the experimental design with the help of Design-Expert software®. Statistical significance of the selected model and the regression coefficients were estimated by multiple regressions using ANOVA. For each response, the model which generated a higher F value was selected as the best fitted model. The accuracy and adequacy of the model was determined by measuring the $R^2$ value, which indicates the 'goodness of fit' of the model to the experimental results. The positive coefficient in polynomial equation suggests that the response varies directly with successive increase in the value of independent variables (i.e., synergistic effect), whereas the negative sign indicates that the response decreases with successive increase the value of independent variables (i.e., inverse effect). The

absolute value of the co-efficient indicates the magnitude of effect of the independent variables on the response variable; the higher the value the higher the magnitude [179, 211-213].

**Table 5.7 Box-Behnken experimental design showing experimental runs with independent variables and their measured responses: particle size ($Y_1$), encapsulation efficiency ($Y_2$), and PDI ($Y_3$) of CS-PNs**

| Run No. | Independent variables | | | Dependent variables | | |
|---|---|---|---|---|---|---|
| | $X_1$ | $X_2$ | $X_3$ | $Y_1$ | $Y_2$ | $Y_3$ |
| **Factorial Points** | | | | | | |
| 1 | -1 | -1 | 0 | 278.6 ± 4.1 | 27.3 ± 0.4 | 0.293 ± 0.048 |
| 2 | 1 | -1 | 0 | 339.1 ± 2.7 | 41.5 ± 1.7 | 0.531 ± 0.021 |
| 3 | -1 | 1 | 0 | 249.8 ± 6.8 | 25.1 ± 1.6 | 0.194 ± 0.074 |
| 4 | 1 | 1 | 0 | 311.4 ± 3.9 | 38.2 ± 2.4 | 0.467 ± 0.061 |
| 5 | -1 | 0 | -1 | 282.9 ± 12.4 | 29.1 ± 1.3 | 0.300 ± 0.053 |
| 6 | 1 | 0 | -1 | 356.4 ± 10.3 | 43.6 ± 2.7 | 0.512 ± 0.034 |
| 7 | -1 | 0 | 1 | 256.8 ± 7.8 | 24.1 ± 0.8 | 0.158 ± 0.039 |
| 8 | 1 | 0 | 1 | 305.1 ± 2.1 | 38.3 ± 1.6 | 0.425 ± 0.042 |
| 9 | 0 | -1 | -1 | 324.1 ± 5.7 | 38.64 ± 0.2 | 0.468 ± 0.071 |
| 10 | 0 | 1 | -1 | 295.9 ± 1.5 | 35.7 ± 2.1 | 0.369 ± 0.064 |
| 11 | 0 | -1 | 1 | 296.8 ± 4.6 | 36.1 ± 1.3 | 0.356 ± 0.012 |
| 12 | 0 | 1 | 1 | 261.1 ± 3.1 | 28.75 ± 1.7 | 0.257 ± 0.039 |
| **Centre Points** | | | | | | |
| 13 | 0 | 0 | 0 | 292 ± 6.9 | 37.4 ± 0.8 | 0.362 ± 0.038 |
| 14 | 0 | 0 | 0 | 296.1 ± 7.1 | 37.5 ± 0.9 | 0.350 ± 0.047 |
| 15 | 0 | 0 | 0 | 297.8 ± 8.7 | 38.7 ± 1.2 | 0.367 ± 0.086 |
| 16 | 0 | 0 | 0 | 295.9 ± 9.2 | 38.6 ± 1.5 | 0.354 ± 0.032 |
| 17 | 0 | 0 | 0 | 294.7 ± 7.6 | 38.2 ± 0.4 | 0.361 ± 0.057 |

*All data are shown as mean ±S.D; n=3*

3D response surface plots were constructed using respective polynomial equations to reveal the interactive effect of any two independent variables on dependent variable graphically, keeping third one at a constant level. The relationships between the dependent variable and the independent variables were also visualized by 2D contour plots for understanding the relative influence of the independent variable along with in combinations [179, 180, 182]. The mathematical relationships of independent variables' coefficients along with corresponding *p*-values for the dependent variables obtained by regression analysis are summarized in Table 6.8. *p*-value less than 0.05 was considered as statistically significance.

**Table 5.8 Statistical analysis of dependent variables of Box-Behnken experimental design along with estimated regression coefficients and associated *p* values**

| Factor | $Y_1$ = Particle size | | $Y_2$ = EE | | $Y_3$ = PDI | |
|---|---|---|---|---|---|---|
| | **Coefficient** | ***p* Value** | **Coefficient** | ***p* Value** | **Coefficient** | ***p* Value** |
| Intercept | 295.30 | < 0.0001 | 38.08 | < 0.0001 | 0.36 | < 0.0001 |
| $X_1$ | 30.49 | < 0.0001 | 7.00 | < 0.0001 | 0.12 | < 0.0001 |
| $X_2$ | -15.05 | < 0.0001 | -1.97 | 0.0002 | -0.045 | < 0.0001 |
| $X_3$ | -17.44 | < 0.0001 | -2.47 | < 0.0001 | -0.057 | < 0.0001 |
| $X_1X_2$ | 0.27 | 0.8495 | -0.28 | 0.5220 | -0.0087 | 0.0694 |
| $X_1X_3$ | -6.30 | 0.0028 | -0.075 | 0.8594 | 0.014 | 0.0120 |
| $X_2X_3$ | -1.87 | 0.2213 | -1.10 | 0.0306 | 0.000 | 1.0000 |
| $X_1^2$ | 2.62 | 0.0952 | -3.04 | 0.0001 | -0.0006 | 0.8749 |
| $X_2^2$ | -3.20 | 0.0510 | -2.02 | 0.0014 | 0.013 | 0.0133 |
| $X_3^2$ | 2.38 | 0.1246 | -1.27 | 0.0154 | -0.0094 | 0.0502 |

#### 5.2.2.2.1 Influence of Independent variables on particle size

The particle size of the prepared CS-PNs was obtained in the range of 249.8 ± 6.8 nm to 356.4 ± 10.3 nm by varying the levels of different independent variables in their limits. The quadratic model was selected for the statistical analysis of influence of independent variables on particle size based on the lack of fit test as shown in Table 5.9.

**Table 5.9 Statistical analysis results of lack of fit for particle size, EE and PDI of CS-PNs**

| Source | Sum of Squares | df | Mean Square | F Value | p-value Prob > F | |
|---|---|---|---|---|---|---|
| **Particle size** | | | | | | |
| Linear | 301.09 | 9 | 33.45 | 7.23 | 0.0362 | - |
| 2FI | 127.96 | 6 | 21.33 | 4.61 | 0.0804 | - |
| Quadratic | 36.12 | 3 | 12.04 | 2.60 | 0.1890 | Suggested |
| Cubic | 0.000 | 0 | - | - | - | Aliased |
| Pure Error | 18.50 | 4 | 4.63 | - | - | - |
| **Encapsulation efficiency** | | | | | | |
| Linear | 77.39 | 9 | 8.60 | 23.43 | 0.0041 | - |
| 2FI | 72.21 | 6 | 12.03 | 32.79 | 0.0023 | - |
| Quadratic | 3.20 | 3 | 1.07 | 2.90 | 0.1650 | Suggested |
| Cubic | 0.000 | 0 | - | - | - | Aliased |
| Pure Error | 1.47 | 4 | 0.37 | - | - | - |
| **PDI** | | | | | | |
| Linear | 0.002391 | 9 | 0.00026 | 5.81 | 0.0528 | - |
| 2FI | 0.001328 | 6 | 0.00022 | 4.84 | 0.0743 | - |
| Quadratic | 0.000284 | 3 | 0.00009 | 2.07 | 0.2465 | Suggested |
| Cubic | 0.000 | 0 | - | - | - | Aliased |
| Pure Error | 0.000182 | 4 | 0.00004 | - | - | - |

The second-order polynomial equation (Eq (5.11)) describing an empirical relationship between particle size ($Y_1$) and independent variables, generated by multiple linear regressions can be given as follows in terms of coded variables:

$$Y_1 = 295.30 + 30.49X_1 – 15.05X_2 – 17.44X_3 – 6.30X_1X_3 \quad \text{Eq (5.11)}$$

Non-significant lack of fit value ($p$=0.1890; $p$>0.05) with F-value of 2.60 indicated that quadratic model is best fit to the independent variables for significantly describing the effect on the particle size. The high $R^2$ value (0.9954) implied the existence of reasonable agreement between predicted and experimental values for explaining the 99.54% variation in particle size. The minimal difference between predicted $R^2$ (0.9494) and adjusted $R^2$ (0.9896) value suggested the adequacy of the selected model for the prediction of response. The value of adequate precision was found to be 49.297 (greater than 4 is desirable), suggesting an adequate signal to measure the signal independent of noise. Further, low value for coefficient of variation (0.94 %) indicated high degree of precision and reliability of the model. Hence, this selected quadratic model can be used to navigate the design space [54, 179, 212].

Except concentration of polymer ($X_1$), all other model terms have significant negative effect on particle size. Also higher coefficient value (30.49) of concentration of polymer ($X_1$) suggested that it had most significant effect on particle size followed by organic phase/aqueous phase ratio ($X_3$) and concentration of surfactant ($X_2$). While in case of the interaction effects between different independent variables, only concentration of polymer and organic phase/aqueous phase ratio ($X_1X_3$) had combined significant effect on particle size. It is visually discerned from 3D response surface plots and 2D contour plots as shown in Figure 5.5.

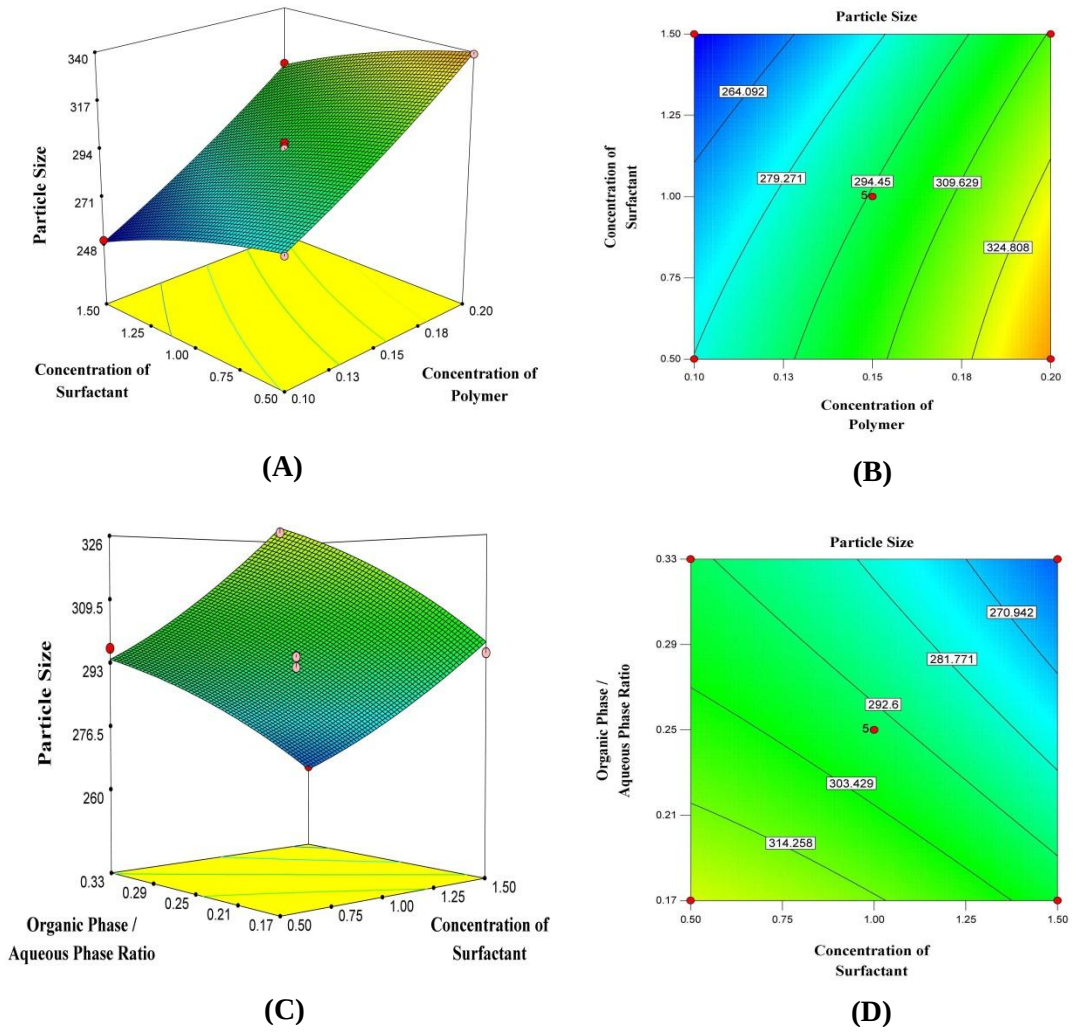


**Figure 5.5 3D response surface plots (A), (C) and 2D contour plots (B), (D) showing the effect of independent variables (concentration of polymer, concentration of surfactant and organic phase/aqueous phase ratio) on particle size of CS-PNs.**

The concentration of polymer ($X_1$) positively affects the particle size of CS-PNs owing to its direct influence on the viscosity. An increase in the polymer concentration raises the polymer-polymer interactions coupled with viscosity of the dispersed phase which reduces stirring capacity, resulting in formation of poor dispersion and thereby, coarse emulsion that builds larger size polymeric particles during the diffusion process. Moreover, the density difference between two phases at higher polymer concentration retards the faster diffusion of organic solvent into

external aqueous phase and also increases the collisions between particles due to enhanced contact and thus, produces larger coacervates [182, 214].

Alternatively, the monotonous decrement in particle size was observed with an increase in surfactant concentration ($X_2$) that might be due to reduction of interfacial tension between aqueous and organic phase, which would have resulted in smaller size particles. Additionally, higher surfactant concentration also offers the interfacial stabilization against coalescence to smaller particles [182, 215]. Likewise, organic phase/aqueous phase ratio ($X_3$) holds inverse proportionality with the particle size. Increase in organic to aqueous phase ratio leads to decrease in particle size by preventing the droplet aggregation as a result of presence of the large amount of organic solvent, which decreases the polymer concentration as well as viscosity and imparts higher shear stress to break down the emulsion droplets [54, 214].

**5.2.2.2.2 Influence of Independent variables on encapsulation efficiency**

For different variable level combination, the EE of CS-PNs was found in the range of 24.1 $\pm$ 0.8 % to 43.6 $\pm$ 2.7 %. The quadratic model was selected for the statistical analysis of influence of independent variables on EE of CS-PNs based on the lack of fit test as shown in Table 5.9. The effect of the independent variables on EE ($Y_2$) can be explained by the following second-order quadratic equation (Eq (5.12)) in terms of coded variables.

$$Y_2 = 38.08 + 7.00X_1 - 1.97X_2 - 2.47X_3 - 0.075X_2X_3 - 3.04X_1^2 - 2.02X_2^2 - 1.27X_3^2 \quad \text{Eq (5.12)}$$

Non-significant lack of fit value ($p$=0.1650; $p$>0.05) with F-value of 2.90 indicated that quadratic model is best fit to the independent variables for significantly describing the influence on the EE. Good correlation between experimental and

predicted values was noticed as revealed by $R^2$ value of 0.9915. The minimal difference between predicted $R^2$ (0.9031) and adjusted $R^2$ (0.9807) value indicated the adequacy of the selected model for the prediction of response. The value of adequate precision was found to be 30.348 (greater than 4 is desirable), suggesting an adequate signal to measure the signal independent of noise. Further, low value for coefficient of variation (2.32 %) indicated high degree of precision and reliability of the model. Thus, the present quadratic model for EE can be used to navigate the design space [54, 179, 212].

Except concentration of polymer ($X_1$), all other model terms have significant negative effect on EE. Also higher coefficient value (7.00) of concentration of polymer ($X_1$) suggested that it had most significant effect on EE followed by organic phase/aqueous phase ratio ($X_3$) and concentration of surfactant ($X_2$). While in case of the interaction effects between different independent variables, only concentration of surfactant and organic phase/aqueous phase ratio ($X_2X_3$) had combined significant effect on EE. However, effect of independent variables on EE is lower than the effect on particle size. This is because of the lower coefficient value of the main effects and interaction terms in the polynomial equation of EE compared with the polynomial equation of particle size [54, 179]. 3D response surface plots and 2D contour plots portraying the effect of independent variables on EE are shown in Figure 5.6.

Concentration of polymer ($X_1$) influences positively on the EE owing to its direct effect on viscosity. Higher polymer concentration offers viscous diffusional barrier, which curtails the drug diffusion into external aqueous phase and thereby, provides higher encapsulation. Moreover, increased particle size at higher polymer concentration also favors high EE by increasing the diffusional path length [216]. Conversely, higher surfactant concentration ($X_2$) lowers EE by reducing interfacial

tension, which promotes partition and hence, solubility of drug into aqueous phase during preparation [208, 217]. Similarly, reduced EE with an increase in organic phase/aqueous phase ratio ($X_3$) was noticed due to substantial reduction in viscus diffusional barrier, which would have favored the drug partition in external aqueous phase [218].

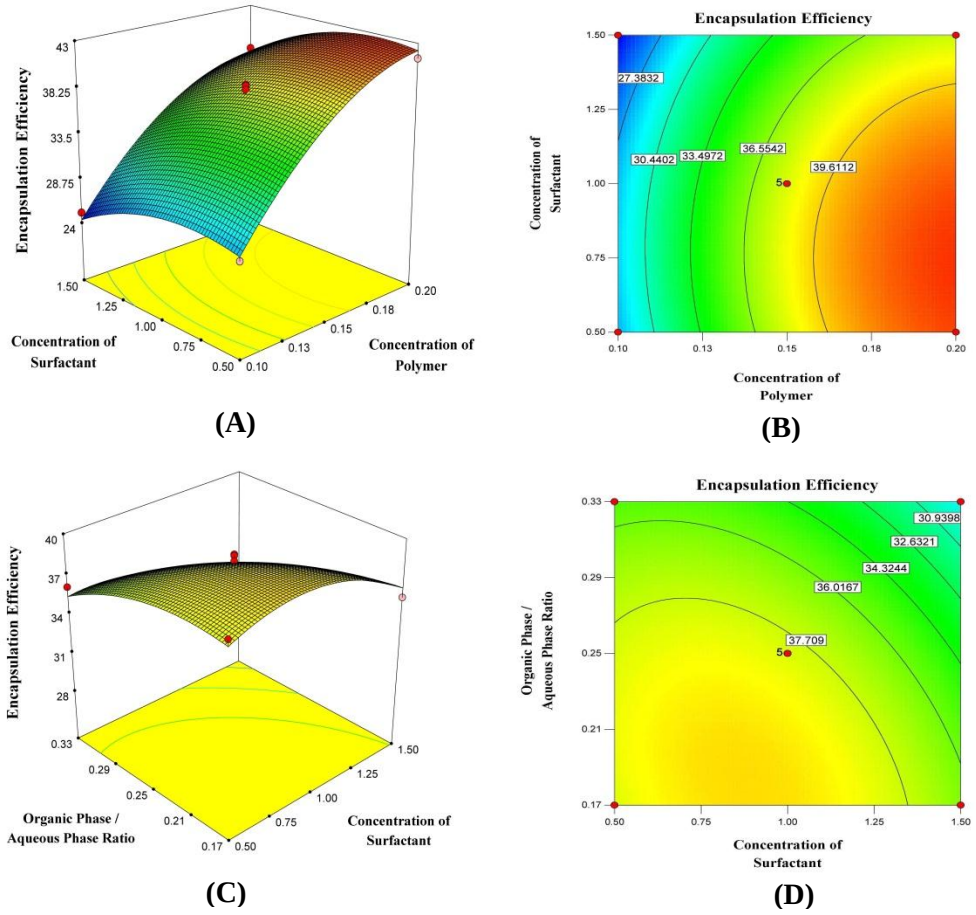


**Figure 5.6 3D response surface plots (A), (C) and 2D contour plots (B), (D) showing the effect of independent variables (concentration of polymer, concentration of surfactant and organic phase/aqueous phase ratio) on encapsulation efficiency of CS-PNs.**

### 5.2.2.2.3 Influence of independent variables on polydispersity index

The CS-NPs exhibited relatively narrow particle size distribution, as indicated by relatively low PDI values. The particle size distribution of CS-PNs was obtained in

the range of 0.158 ± 0.039 to 0.531 ± 0.021 for selected level combination of different variables. Low PDI values nearer to 0 indicate the relative homogenous nature of the dispersion. The quadratic model was selected for the statistical analysis of influence of independent variables on PDI based on the lack of fit test as shown in Table 5.9. The second-order polynomial equation (Eq (5.13)) for PDI ($Y_3$) in terms of independent variables was obtained as follows in terms of coded variables.

$$Y_3 = 0.36 + 0.12X_1 - 0.045X_2 - 0.057X_3 + 0.014X_1X_3 + 0.013X_2^2 \qquad \text{Eq (5.13)}$$

The F-value of 2.07 with the absence of lack of fit value ($p$=0.2465; $p$>0.05) for quadratic model proves the excellent adequacy for significantly describing the effect of independent variables on the PDI. The higher $R^2$ value of 0.9972 suggests that 99.72% of variation in PDI was best explained by the formulation variables. The minimal difference between predicted $R^2$ (0.9711) and adjusted $R^2$ (0.9936) value suggested the adequacy of the selected model for the prediction of response. The value of adequate precision was found to be 60.137 (greater than 4 is desirable), suggesting an adequate signal to measure the signal independent of noise. Further, low value for coefficient of variation (2.27 %) indicated high degree of precision and reliability of the model. Hence, the quadratic model can be considered for navigating the design space [54, 179, 212].

Except concentration of polymer ($X_1$), main effect of all other model terms has significant negative effect on PDI. Also higher coefficient value (0.12) of concentration of polymer ($X_1$) suggested that it had most significant effect on PDI followed by organic phase/aqueous phase ratio ($X_3$) and concentration of surfactant ($X_2$). While in case of the interactive effects between different independent variables, only concentration of polymer and organic phase/aqueous phase ratio ($X_1X_3$) had

combined significant effect on PDI. However, effect of independent variables on PDI is lowest than the effect on particle size and EE. This is because of the lower coefficient value of the main effects and interaction terms in the polynomial equation of PDI compared with the polynomial equation of particle size and EE [54, 179]. It is visually discerned from 3D response surface plots and 2D contour plots as shown in Figure 5.7.

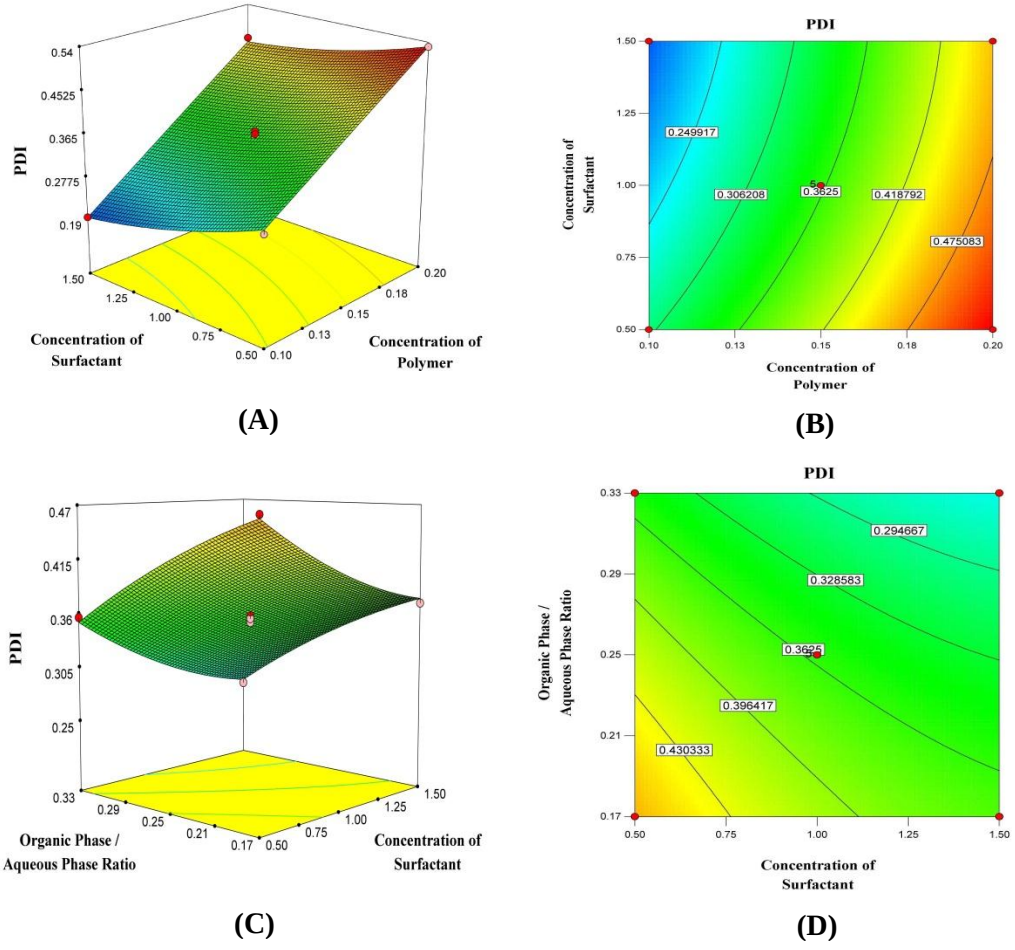


**Figure 5.7 3D response surface plots (A), (C) and 2D contour plots (B), (D) showing the effect of independent variables (concentration of polymer, concentration of surfactant and organic phase/aqueous phase ratio) on PDI of CS-PNs.**

The increase in PDI value was noticed with an increase in polymer concentration ($X_1$) might be attributed to formation of coarse dispersion due to the absence of sufficient

shear stress to overcome the resistive viscous forces, which directly affects the emulsification efficiency and generates different-sized particles. Additionally, the lack of sufficient surfactant concentration for stabilization of newly formed particles also enhances the particle size distribution [214]. Whereas enhanced surfactant concentration ($X_2$) and organic phase/aqueous phase ratio ($X_3$) decreases PDI by reducing interfacial tension as well as polymer concentration which in turn enforces monodispersity [39, 54].

#### 5.2.2.2.4 Optimization of CS-PNs using desirability function

Optimization of formulation by considering all the objectives at a time is difficult because of opposite effect of various independent variables. The optimum level of one independent variable might result in an inverse effect for other independent variable. Hence, the numerical optimization was performed by employing desirability approach upon application of constraints to the three different dependent variables. The levels of different independent variable which would yield maximum EE with minimum particle size and PDI were determined using Design-Expert® software. In order to optimize and validate the predictive power of the model, the CS-PNs were prepared under the optimal conditions by considering the predicted levels of respective independent variables. Table 5.10 shows the predicted values of dependent variables and levels of independent variables along with the experimental results. The desirability of the optimized CS-PNs was 0.629. The close proximity with low percentage of bias between predicted results and experimental results reaffirmed the reliability of prognostic ability of Box-Behnken experimental design for statistical optimization of desirable CS-PNs [39, 179, 182, 183]. Optimized CS-PNs were further selected for various *in-vitro* and *in-vivo* characterizations.

**Table 5.10 Comparison of experimental and predicted values of optimized CS-PNs with its desirability generated by Design expert®**

| Independent variables | Optimized levels |
|---|---|
| Concentration of polymer ($X_1$) | 0.14 % w/v |
| Concentration of surfactant ($X_2$) | 1.13 % w/v |
| Organic phase/Aqueous phase ratio ($X_3$) | 0.30 |

| Results | | | |
|---|---|---|---|
| | **Experimental values** | **Predicted values** | **% Bias*** |
| Particle size (nm) | 262.4 ± 7.6 | 275.48 | 4.74 |
| Encapsulation efficiency (%) | 34.26 ± 1.3 | 33.64 | -1.84 |
| Polydispersity index (PDI) | 0.271 ± 0.02 | 0.280 | 3.21 |
| Overall Desirability | 0.629 | | |
| Drug loading (%) | 4.1 ± 0.11 | | |
| Zeta potential (mV) | (-) 19.3 ± 1.7 | | |

**Bias was calculated as [(predicted value-experimental value)/predicted value] X 100;*
*All results are shown as mean ±S.D; n=3*

### 5.2.3 Characterizations of CS-PNs

#### 5.2.3.1 Solid state characterizations

##### 5.2.3.1.1 Fourier transform infrared spectroscopy (FTIR) study

FTIR study was performed in order to identify the significant change, if occurs during the encapsulation of CS inside the nanoparticles. The FTIR spectra for pure CS, PLGA, PVA and optimized CS-PNs are shown in Figure 5.8. As depicted in Figure 5.8 (a), FTIR spectra of CS showed the basic peaks at 1639.54 $cm^{-1}$ and 3416 $cm^{-1}$, assigned to the C=O and O-H stretching as well as characteristic peaks at 2880 $cm^{-1}$ (C-H alkane), 1477 $cm^{-1}$ (aromatic C-H), 1573 $cm^{-1}$ and 1410 $cm^{-1}$ (asymmetric and

symmetric $COO^{-}$). Moreover, the vibrations within a molecule were noticed through the large number of characteristic bands in fingerprint region (1400–600 $cm^{-1}$) [43, 45].

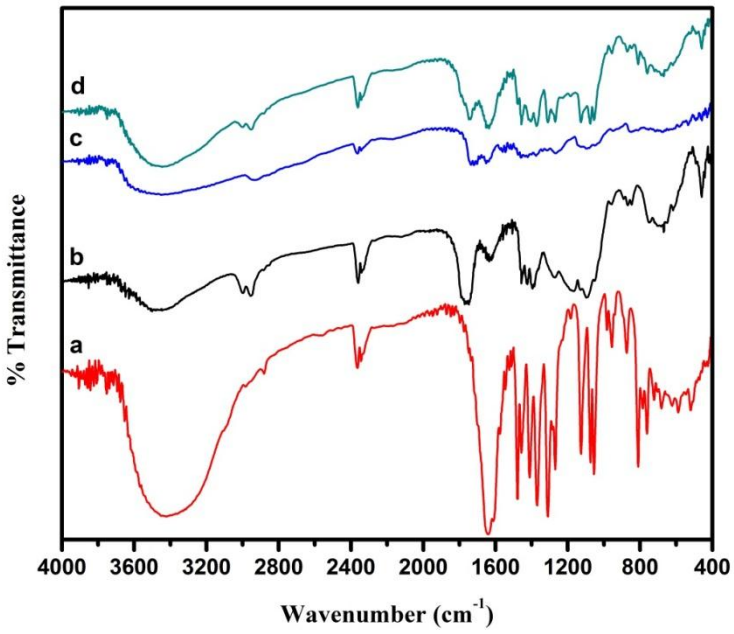


**Figure 5.8 FTIR spectra of (a) CS, (b) PLGA, (c) PVA and (d) optimized CS-PNs**

FTIR spectra of PLGA showed various bands at 1748.12 $cm^{-1}$ (C=O stretching), 1194.25 $cm^{-1}$ (C-O stretching), 2948.47 $cm^{-1}$ (C-H stretching) and broad bands between 3200-3600 $cm^{-1}$ owing to its terminal hydroxyl group [205]. In FTIR spectra of optimized CS-PNs (Figure 5.8 (c)), the characteristic band at 3416 $cm^{-1}$ becomes wider, which indicates the enhancement in the hydrogen bonding of CS [220]. Moreover, all the characteristic peaks of CS were observed at nearly same wavenumber as appeared in pure CS with reduced intensity, ensuring the presence and successful encapsulation of CS inside the matrix of the nanoparticles without any interaction or modification during the encapsulation process [221].

### 5.2.3.1.2 Differential scanning calorimetry (DSC) study

DSC is a useful technique to investigate the physicochemical state of the drug molecule inside the nanoparticles by understanding the melting and recrystallization behaviour of drug molecule [222, 223]. DSC thermogram of pure CS, PLGA, PVA and CS-PNs are depicted in Figure 5.9. The pure CS displayed sharp endothermic peak at 264 $^{o}$C corresponding to its melting point which gave an indication about its crystalline behaviour. Further, any peaks due to release of absorbed moisture or nonstructural water as well as solid state transitions were not identified [149, 210]. PLGA exhibited sharp endothermic peak at 65 $^{o}$C.

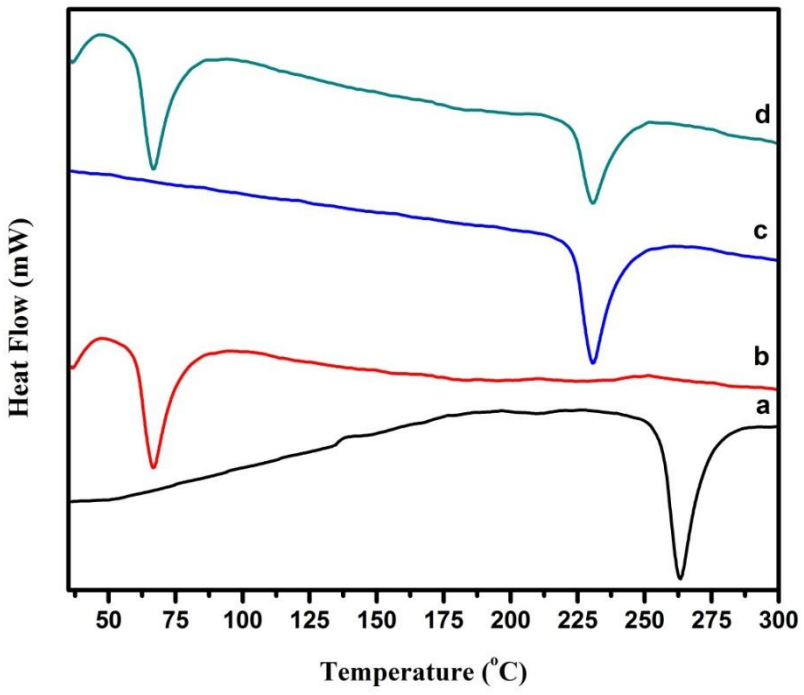


**Figure 5.9 DSC thermograms of (a) CS, (b) PLGA, (c) PVA and (d) optimized CS-PNs.**

In case of DSC thermogram of CS-PNs, the crystalline endothermic peak of CS was completely vanished, which indicates that the physical state transformation is taken

place during the encapsulation process and CS is dispersed in an amorphous molecular dispersion or solid solution state inside the matrix of polymeric nanoparticles (Figure 5.9 (d)). Endothermic peak at 226 $^{o}$C was due to melting of PVA at corresponding temperature (Figure 5.9 (c)). However, no any pronounced effect in the thermal behaviour pattern of PLGA was observed. Hence, it seemed that polymer matrix has entirely covered the CS in an amorphous form during the encapsulation process [207, 210, 224].

**5.2.3.1.3 Powder X-ray diffractometry (PXRD) study**

PXRD is a non-destructive analytical technique which provides the information regarding the physical state or crystal lattice arrangement of drug in the powder formulation [225]. Powder X-ray diffractogarms of PLGA, pure CS, PVA, their physical mixture and optimized CS-PNs are depicted in Figure 5.10. The powder X-ray diffraction pattern of pure CS exhibited its traits of highly crystalline nature by numerous, distinct sharp diffraction peaks, observed at a 2θ value of 8$^{o}$, 9.83$^{o}$, 11.5$^{o}$, 14$^{o}$, 16.9$^{o}$, 19.7$^{o}$, 24.3$^{o}$, 26.6$^{o}$ and various minor peaks up to 35$^{o}$ as illustrated in Figure 5.10 (b) [45, 149]. The powder X-ray diffractograms of PLGA and PVA showed small diffuse peaks with broad halo [39, 205]. The crystallinity of the CS was retained in the physical mixture of CS along with PLGA and PVA as observed by its sharp peaks in diffractogram of the physical mixture. Since PLGA and PVA exhibited no any characteristic diffraction peaks, the crystalline peaks must be originated from the crystalline region of CS due to absence of any interaction (Figure 5.10 (d)). Whereas, PXRD pattern of optimized CS-PNs showed more of an amorphous nature as compared to pure CS due to stifling of its diffraction intensity with greater disarray as shown in Figure 5.10 (e).

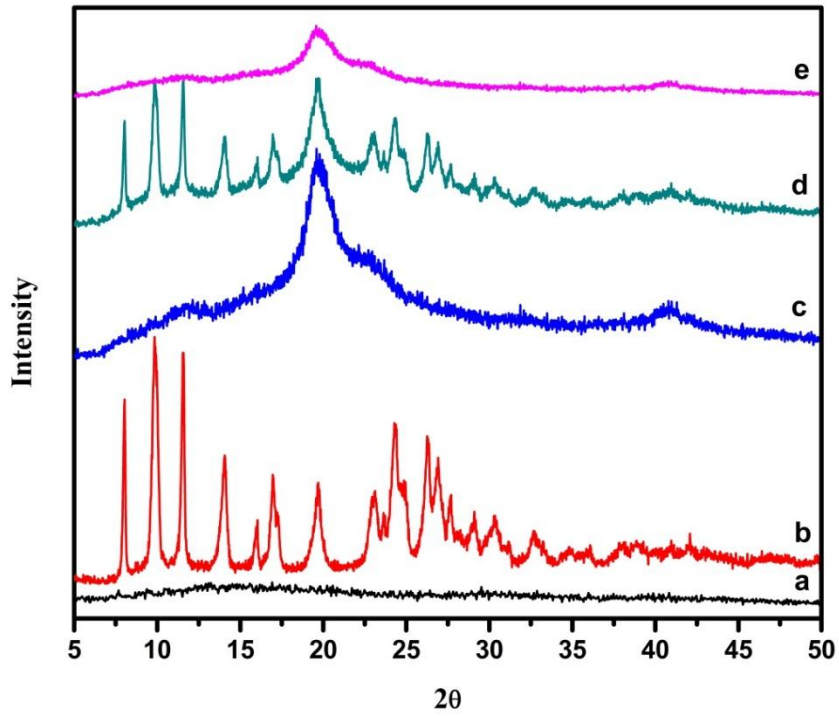


**Figure 5.10 PXRD patterns of (a) PLGA, (b) CS, (c) PVA, (d) physical mixture and (e) optimized CS-PNs**

The absence of intense, crystalline peaks of CS in optimized CS-PNs with high noise suggested the physical state deformation from crystalline state to amorphous state upon encapsulation inside the polymer matrix [207, 210, 226]. PXRD results are in good agreement with the results demonstrated by DSC, confirming the homogeneous and complete encapsulation of CS inside the polymeric matrix of the nanoparticles [39, 45, 224].

### 5.2.3.2 Shape and surface morphology

#### 5.2.3.2.1 High resolution transmission electron microscopy (HR-TEM)

The shape and surface morphology of the optimized CS-PNs was examined by employing HR-TEM. The HR-TEM micrographs (Figure 5.11 (A)) revealed that the developed CS-PNs were well separated and nearly spherical in shape having

homogeneous and unimodal size distribution. The external surface morphology of CS-PNs exhibited smooth surface without any visible pores or crevices. The particle size obtained by HR-TEM was well correlated with the particle size measured by dynamic light scattering technique, in which most of them are smaller than 300 nm.

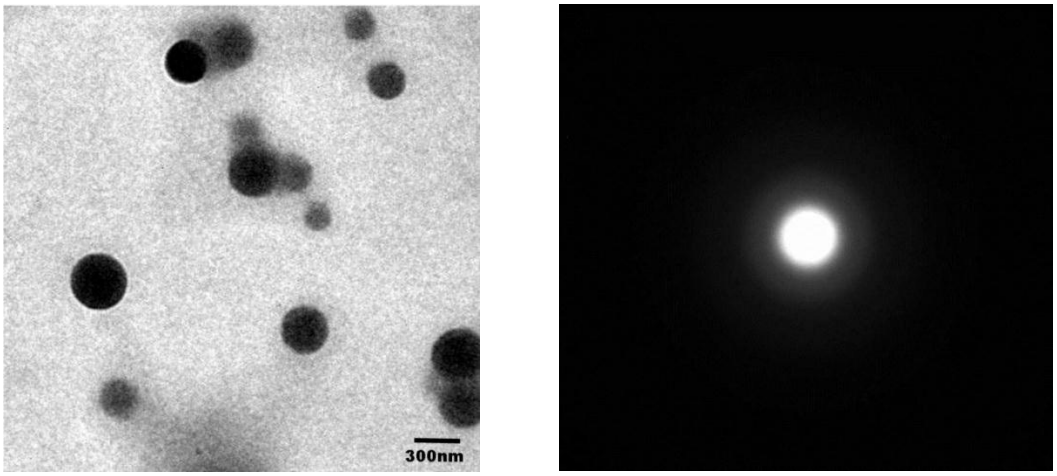


**(A)** **(B)**

**Figure 5.11 (A) HR-TEM image of optimized CS-PNs and (B) Electron diffraction pattern of optimized CS-PNs**

Further, the physical state of CS inside the polymeric matrix was studied by electron diffraction (ED) pattern. The ED pattern (Figure 5.11 (B)) obtained by visualizing CS-PNs revealed the existence of smooth diffraction halo without any bright spots in the circular ring pattern, indicating that CS was encapsulated homogeneously as an amorphous form inside the nanoparticles [39, 198, 226], which further substantiates the inference deduced from DSC and PXRD results.

#### 5.2.3.2.2 Atomic force microscopy (AFM)

The surface morphology of optimized CS-PNs was further confirmed by AFM study. The topographic and 3D AFM micrographs of CS-PNs, generated by the atomic level

interaction between a sharp probing tip and the surface of CS-PNs with a spatial resolution up to 0.01 nm, are depicted in Figure 5.12 (A) & (B).

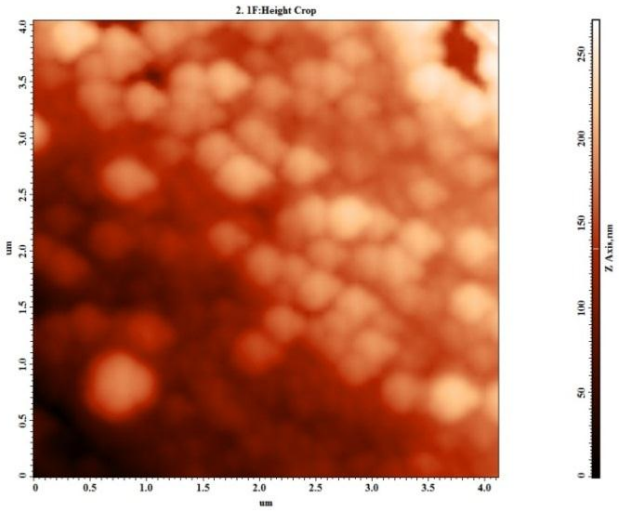


**(A)**

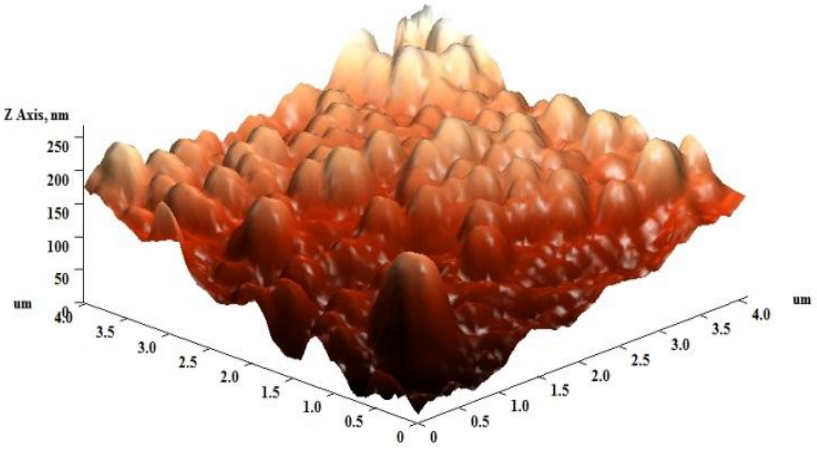


**(B)**

**Figure 5.12 AFM images of optimized CS-PNs (A) 2D micrograph and (B) corresponding 3D micrographs.**

The particle size and surface morphology revealed by AFM was in accordance with the results of HR-TEM study. AFM images generated by direct analysis of originally hydrated CS-PNs sample, demonstrated uniform spherical shaped CS-PNs having smooth surface without any visible crevices or pores. AFM micrographs displayed the well dispersed CS-PNs in the nanometric size range with low polydispersity. The probable reason for smooth surface could be the covering of surfactant molecules over the external surface of polymeric matrix of nanoparticles, which has resealed the pores or crevices generated by the diffusion of organic solvent during the preparation [23, 188].

#### 5.2.3.3 *In-vitro* drug release study

*In-vitro* drug release profile of CS from CS-PNs showed the biphasic release pattern in phosphate buffer pH 7.4 as illustrated in Figure 5.13. The optimized CS-PNs exhibited around 90% drug release at the end of 24 hr. The surface adsorbed CS showed an initial burst release (nearly 19% drug release) within 1hr due to faster diffusion followed by extended release over 24 hr through slower hydration and polymer swelling (Table 5.11). Hydration causes substantial increment in the diffusional path length, which eventually slowdowns the diffusion of drug molecules form the nanoparticles [227]. Additionally, the extended release behaviour of CS was also correlated to the homogeneous encapsulation within the nanoparticles, which decelerates the faster immobilization from polymeric matrix and controls the release. These results indicated that the release of CS from polymeric nanoparticles was mainly governed by a combination of process, i.e., drug diffusion and polymer chain relaxation during the polymer swelling [36, 49, 198].

**Table 5.11 *In-vitro* drug release data of the optimized CS-PNs in phosphate buffer pH 7.4.**

| Time (hr) | Cumulative % drug release |
|---|---|
| 0 | 0 |
| 1 | 19.76 ± 1.31 |
| 2 | 24.02 ± 0.84 |
| 3 | 27.91 ± 0.55 |
| 4 | 32.63 ± 0.69 |
| 5 | 35.69 ± 0.84 |
| 6 | 40.13 ± 1.54 |
| 7 | 45.69 ± 2.46 |
| 8 | 50.41 ± 1.67 |
| 10 | 56.52 ± 1.15 |
| 12 | 64.86 ± 3.24 |
| 18 | 71.80 ± 1.25 |
| 24 | 89.02 ± 1.78 |

*All values reported are mean ± SD, (n=3)*

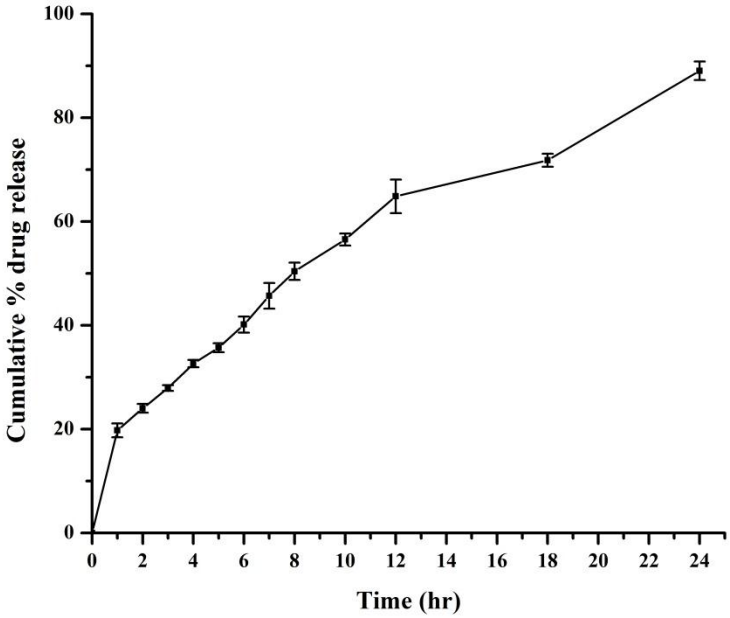


**Figure 5.13 *In-vitro* drug release profile of optimized CS-PNs in phosphate buffer pH 7.4 (vertical bar represents ± S.D; n=3)**

Furthermore, the release kinetics and mechanism was determined by fitting different release kinetic models (i.e., zero order, first order, Higuchi model and Korsmeyer-Peppas model) to the *in-vitro* drug release profile of CS-PNs. Results of *in-vitro* release kinetic analysis suggested that the release of CS from CS-PNs was best explained by Higuchi model showing diffusion based release process (highest $R^2$ value compared to other kinetic models as shown in Table 5.12). Further, the release exponent (n) value obtained by fitting Korsmeyer-Peppas model was found to be 0.499, which is suggestive that the drug release occurred through diffusion controlled release process from the polymer matrix based on Fick's law ($n<0.5$ for fickian diffusion) [191, 192]. Hence, it is possible to provide loading dose due to initial burst release followed by maintenance dose due to sustained release by administering CS-PNs, in order to achieve fluctuation free steady state CS plasma level [49].

**Table 5.12 Release kinetic models for simulation of release behaviour of CS from optimized CS-PNs in phosphate buffer pH 7.4**

| Batch | Zero Order | First Order | Higuchi Model | Korsemeyer-Peppas model |
|---|---|---|---|---|
| Optimized CS-PNs | $R^2 = 0.9605$<br>$K_z = 2.998$ | $R^2 = 0.8543$<br>$K_F = 0.0619$ | $R^2 = 0.9865$<br>$K_H = 18.248$ | $R^2 = 0.9796$<br>$K_P = 17.352$<br>$n = 0.499$ |

### 5.2.3.4 Accelerated and real time storage stability study

The ability of any colloidal system to remain stable against environmental changes is of prime requirement to ensure its final performance in terms of its *in-vivo* fate. Nanoparticles have very high tendency to agglomerate owing to their large surface-area-to-volume ratio, which results in the increase in particle size after long periods of storage. Changes in the physical appearance, color, odor, taste, or texture of the

formulation indicate the instability. The stability and intactness of CS-PNs was assessed over a period of 6 month at room temperature (25 $\pm$ 2 $^{o}$C), refrigerated condition (4 $\pm$ 1 $^{o}$C), and accelerated condition (40 $\pm$ 2 $^{o}$C/75 $\pm$ 5 % RH). The physical appearance and physicochemical attributes (i.e., particle size, EE and PDI) were chosen as stability indicating parameters. The changes in the physicochemical properties of the CS-PNs during the stability study over the period of 6 months are depicted in Figure 5.14.

There was no any significant noticeable change in the physical appearance (i.e., lump formation and discoloration) observed at different environmental condition during the study. Depositions formed on the base of container during storage were easily redispersible on mere shaking. Similarly, insignificant ($p$>0.05) change in the particle size, EE and PDI of CS-PNs was observed during the storage at different environmental conditions, suggesting the high stability of CS-PNs to withstand the environmental fluctuations. Hence, the stability study indicated that the developed CS-PNs are physically as well as chemically stable and able to retain their pharmaceutical properties at various environmental conditions for safe and effective long-term use [49, 193, 228, 229].

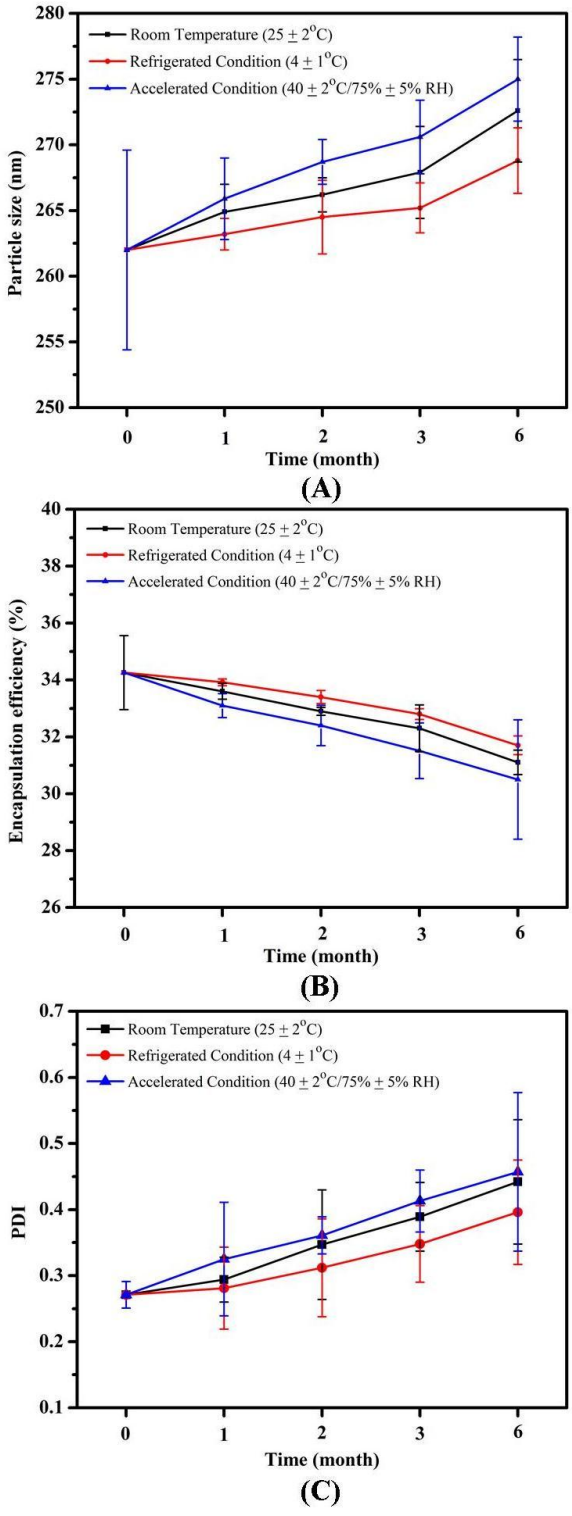


**Figure 5.14 Effect on (A) particle size, (B) encapsulation efficiency and (c) PDI of optimized CS-PNs stored at different environmental conditions over different time interval (vertical bars represent ± SD; n=3)**

### 5.2.3.5 *Ex-vivo* intestinal permeation study

Numerous techniques have been applied for estimating the drug permeation across the GIT. However, *in-vivo* data are most relevant, many different *in-vitro*, *ex-vivo* and *in-vivo* techniques have been employed to evaluate the permeation potential of drug molecules across the GIT of different animals with the help of cell cultures, isolated tissues and side-by-side diffusion chambers, etc. Amongst them, *in-vitro* permeability study using isolated intestinal tissue is most relevant approach to evaluate the permeation of colloidal drug carrier systems by simulating the actual condition stringently. It offers many advantages such as rapid quantification, requirement of fewer animals and involvement of simpler analytical techniques. *In-vitro* intestinal permeation study can be performed by two ways: everted gut-sac method and non-everted gut sac method. In which, non-everted rat intestinal sac method demonstrated good relationship between the in-vitro permeability data and corresponding human absorption data of different drug molecules. Hence, non-everted intestinal sac method was employed for assessing the permeation potential of CS and CS-PNs using rat intestine [107, 230, 231].

The *ex-vivo* intestinal permeation of CS-PNs and CS solution along with their apparent permeability coefficient (Papp) at pH 7.4 is depicted in Figure 5.15. The permeation of CS in the encapsulated form of CS-PNs was significantly increased ($p$<0.05) at each time point; approximately ~4 fold across the rat intestinal tissue compared to CS solution (Table 5.13).

**Table 5.13 *Ex-vivo* permeation data of the CS solution and optimized CS-PNs across rat intestinal membrane**

| Time (min) | Cumulative % drug permeated | |
|---|---|---|
| | CS solution | CS-PNs |
| 0 | 0 | 0 |
| 15 | 1.21 ± 0.039 | 3.33 ± 0.125 |
| 30 | 2.40 ± 0.021 | 4.47 ± 0.318 |
| 45 | 3.33 ± 0.053 | 7.34 ± 0.733 |
| 60 | 4.39 ± 0.052 | 10.69 ± 0.747 |
| 90 | 4.98 ± 0.083 | 19.13 ± 1.237 |
| 120 | 5.71 ± 0.539 | 25.84 ± 1.255 |
| 180 | 6.78 ± 0.504 | 32.71 ± 1.250 |
| 240 | 7.71 ± 0.588 | 41.28 ± 1.723 |

*All values reported are mean ± SD, (n=3)*

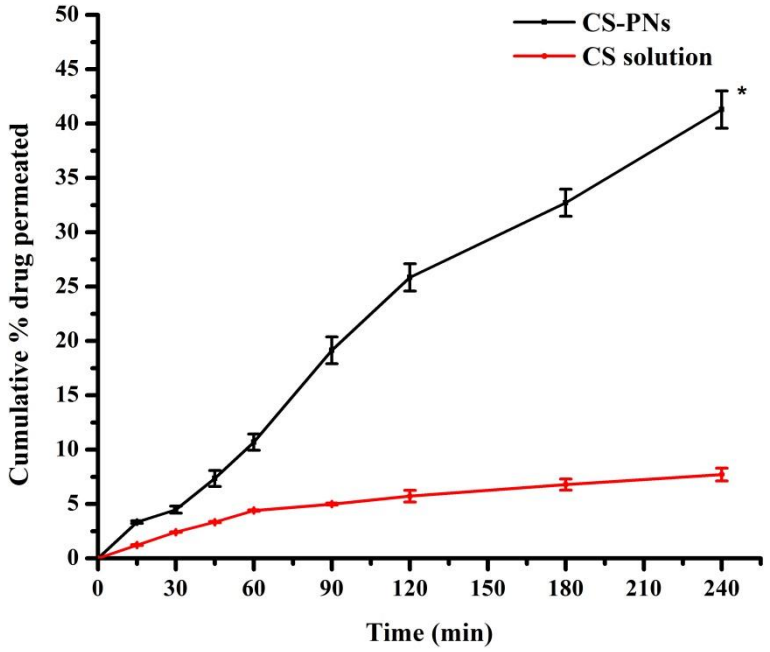


**Figure 5.15 *Ex-vivo* permeation study of CS-PNs and CS solution across rat intestinal membrane. Vertical bars represent ± SD; n=3, *significant at $p<0.05$ compared with CS solution (Unpaired student t-test)**

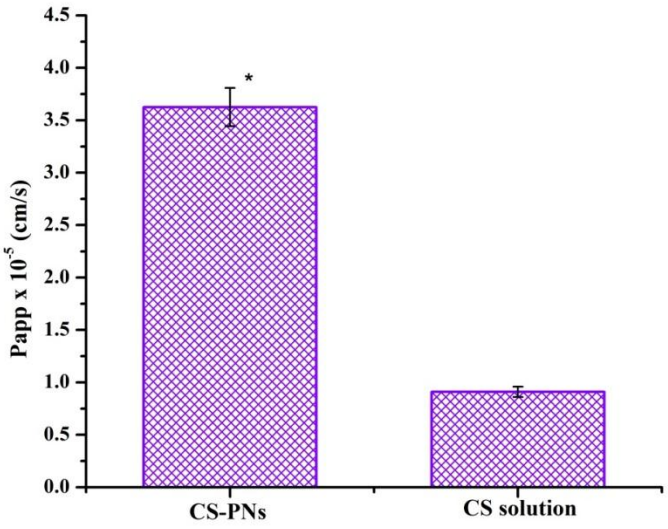


**Figure 5.16 Apparent permeability coefficients (Papp) for CS from CS-PNs and CS solution. Vertical bars represent ± SD; n=3, *significant at *p*<0.05 compared with CS solution (Unpaired student t-test)**

The intestinal permeability coefficients for the CS solution and CS-PNs were found to be 0.909 (± 0.049) × $10^{-5}$ cm/sec and 3.625 (± 0.182) × $10^{-5}$ cm/sec, respectively. The poor permeation of the CS across the rat intestine was due to its highly hydrophilic nature [43, 45]. The permeability enhancement ratio for CS was found to be 3.984 ± 0.36 by developing CS-PNs (Figure 5.16). The higher permeability for the CS-PNs is likely owing to its nanosize structure, which imparts larger specific surface area and their specific absorption mechanisms across the GIT [106, 107]. Moreover, the lipophilic nature of the CS-PNs is also plausible reason for permeation enhancing effect through their selective uptake by M cells of PP in lymphoid tissues as well as endocytosis through enterocytes, which eventually reflected by higher CS concentration in the receptor compartment [24, 39, 232].

### 5.2.3.6 *In-vivo* intestinal uptake study

*In-vivo* intestinal uptake study was performed in rats with an objective to visualize the permeation of CS-PNs across the GIT. FITC tagged CS-PNs were administered orally to the overnight fasted rats. The internalization and distribution of FITC tagged CS-PNs in the intestinal tissue was visualized by CLSM. Figure 5.17 shows confocal microscopic images of cross-sections of rat intestinal tissue, isolated after oral administration of FITC tagged CS-PNs.

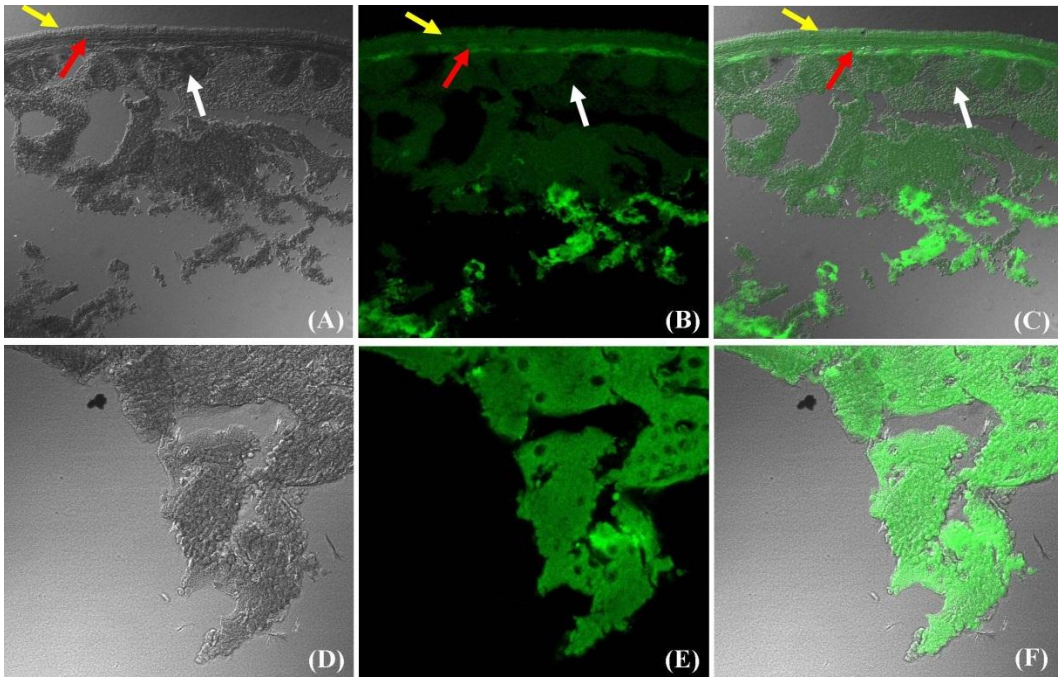


**Figure 5.17 Confocal laser scanning micrographs of rat intestine, showing uptake and transport of FITC tagged CS-PNs into the tissues, underlying the absorptive cells, after 2 hr of oral administration. (A) DIC image; (B) Fluorescent image; and (C) Merge of fluorescent and DIC image scanned at 10× plain. (D) DIC image; (E) Fluorescent image; and (F) Merge of fluorescent and DIC image scanned at 40× plain using emersion oil objective. White, red and yellow arrows indicate the mucosal, submucosal, and muscular regions, respectively**

The strong green fluorescence attributed to FITC was clearly noticed throughout the intestinal tissue, including surface of the villi as well as M-cells of PP, which gave a

confirmation of the effective endocytosis. The absorption of CS-PNs occurs in rat follicular mucosa (PP) as well as non-follicular mucosa (normal enterocytes) as visualized in CLSM images. No fluorescence was observed in the lumen or mucus layer. The distribution and various stage of internalization of CS-PNs suggested that CS-PNs were followed various path of uptake including paracellular, transcellular through enterocytes and endocytosis by M-cells of PP [39, 49, 106, 196]. Additionally, the surfactant used in formulation of CS-PNs (i.e., PVA) also caters mucoadhesivity to CS-PNs which might have helped in improving the residence time of CS-PNs with intestine and resulted in the improved intestinal permeation by facilitating particulate interaction [24]. As CS was encapsulated with the CS-PNs during the absorption across GIT, it would have resulted in the increased permeation. Hence, it can be concluded that nanoparticles play an important role in the facilitating the CS absorption to systemic circulation through the intestinal membrane [233, 234].

#### 5.2.3.7 *In-vivo* pharmacokinetic study

The plasma drug concentration-time profiles obtained after the single dose oral administration of the CS solution and CS-PNs in rats (20 mg/kg) are depicted in Figure 5.18 and Table 5.14. Various pharmacokinetic parameters of pure CS solution and CS-PNs obtained by non-compartmental analysis are summarized in Table 5.15. As can be seen from the mean plasma concentration–time curve, oral administration of CS solution resulted into faster appearance of CS in blood. CS-PNs, on the other hand, displayed entirely different pharmacokinetics.

**Table 5.14 Plasma drug concentration time profile data of CS solution and CS-PNs following single dose oral administration in rats**

| Time (hr) | Plasma concentration of CS (ng/ml) | |
|---|---|---|
| | CS solution | CS-PNs |
| 0 | 0 | 0 |
| 0.25 | 11.42 ± 1.36 | 7.33 ± 1.12 |
| 0.5 | 50.59 ± 4.30 | 39.79 ± 2.23 |
| 1 | 112.23 ± 5.90 | 77.34 ± 2.04 |
| 2 | 70.08 ± 2.86 | 165.32 ± 11.78 |
| 4 | 28.75 ± 2.10 | 99.54 ± 8.55 |
| 8 | ND | 55.97 ± 3.75 |
| 12 | ND | 24.02 ± 2.16 |
| 24 | ND | 7.52 ± 0.98 |

*All values reported are mean ± SEM, (n=6); ND: Not detected*

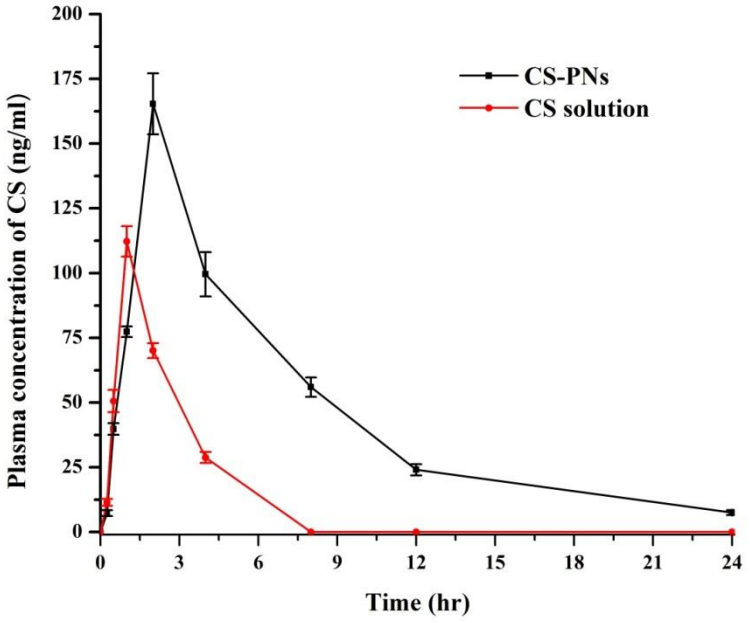


**Figure 5.18 Plasma drug concentration time profile of CS-PNs and CS solution following single dose oral administration in rats; Dose: 20 mg/kg (vertical bars represent ± SEM; n=6)**

**Table 5.15 Pharmacokinetic parameters of CS and CS-PNs following single oral administration in rats (Dose: 20 mg/kg)**

| Parameters | CS solution | CS-PNs |
|---|---|---|
| $C_{max}$ (ng.ml$^{-1}$) | 112.23 ± 5.90 | 165.32 ± 11.78* |
| $T_{max}$ (hr) | 1 (± 0) | 2 (± 0) |
| $AUC_{0-24h}$ (ng.hr.ml$^{-1}$) | 232.16 ± 12.31 | 1077.59 ± 57.42* |
| $AUC_{0-\infty}$ (ng.hr.ml$^{-1}$) | 295.53 ± 17.79 | 1159.41 ± 55.90* |
| $T_{1/2}$ (hr) | 1.52 ± 0.02 | 5.97 ± 0.19* |
| MRT (hr) | 2.79 ± 0.03 | 9.05 ± 0.20* |
| Fr | 1 | 4.69 ± 0.51* |

**significant at p<0.05 compared with CS solution (Unpaired student t-test); All values reported are mean ± SEM, (n=6).*

Non-compartmental analysis of CS plasma concentrations exhibited ~1.47 fold increments in peak plasma drug concentration ($C_{max}$) for CS-PNs with respect to pure CS solution. The higher $C_{max}$ for CS-PNs can be due to enhanced permeation thereby, absorption across GIT by virtue of their smaller size and hydrophobic surfaces [27, 226]. The time required to reach maximum drug concentration ($T_{max}$), half-life ($T_{1/2}$), and observed mean residence time (MRT) obtained with CS-PNs were significantly higher than those obtained with pure CS solution. The plasma level of CS after the oral administration of CS solution was detected only up to 4 hr whereas CS-PNs detected up to 24 hr. The MRT of CS-PNs is about ~3.22 times greater that with CS solution, indicating prolonged stay of CS in body by incorporating into nanoparticles. The $T_{1/2}$ of CS is also increased from ~1.52 hr (CS-solution) to ~5.97 hr (CS-PNs) after oral administration. It might be due to retention of CS-PNs in an intestinal mucosa, which slowly absorbs and releases encapsulated CS over longer period of time thereby, reiterating the potential of CS-PNs as a sustained delivery system [106,

107, 235]. The values of $AUC_{0\text{-}24hr}$ and $AUC_{0\text{-}\infty}$ for CS-PNs were significantly higher ($p$<0.05) compared to pure CS solution, indicating the significant increase in the bioavailability of CS. The relative bioavailability of CS-PNs was found to be ~4.69 fold higher with respect to CS solution upon single dose oral administration. Enhancement of oral bioavailability might be attributed to the nano-sized structure and increased surface area, which would have enhanced systemic absorption of CS-PNs through selective lymphatic uptake by M cells of PP and trancellular transport through enterocytes [23, 106, 107, 236]. Results coupled with confocal microscopic study corroborate well with the findings of *ex-vivo* studies.

#### 5.2.3.8 *In-vivo* mast cell stabilizing activity

Mast cells are type of inflammatory cells, which are predominantly involves in the various allergic conditions. They are available in large numbers in various mucosal tissues of respiratory, gastrointestinal tract, skin, blood vessels and lymphatic vessels, etc. Compound 48/80 is a cationic amphiphile obtained from the condensation of the N-methyl-p-methoxyphenethyamine and formaldehyde. It increases the permeability of lipidic membrane of mast cell by acting as a calcium channel ionophore, which results in mast cell disruption and thereby, release of chemical mediators (i.e., histamine and necrosis factor) from sensitized mast cells [200-202]. The results of mast cell stabilizing activity in the rats are summarized in the Table 5.16. Figure 5.19 shows the degradation of the isolated peritoneal mast cells in different groups, after incubation with the compound 48/80. In the normal control group, isolated peritoneal mast cells showed 10.515 ± 0.8813 % activation. Whereas, positive control group showed 93.033 ± 3.648 % activation of mast cells, upon incubation with compound 48/80. Prophylactic treatment with oral administration of the CS solution (20 mg/kg) and CS-PNs (20 mg/kg) for 7 days in the rats has offered significantly higher ($p$<0.05)

protection against mast cell degranulation and reduced the total number of activated mast cell.

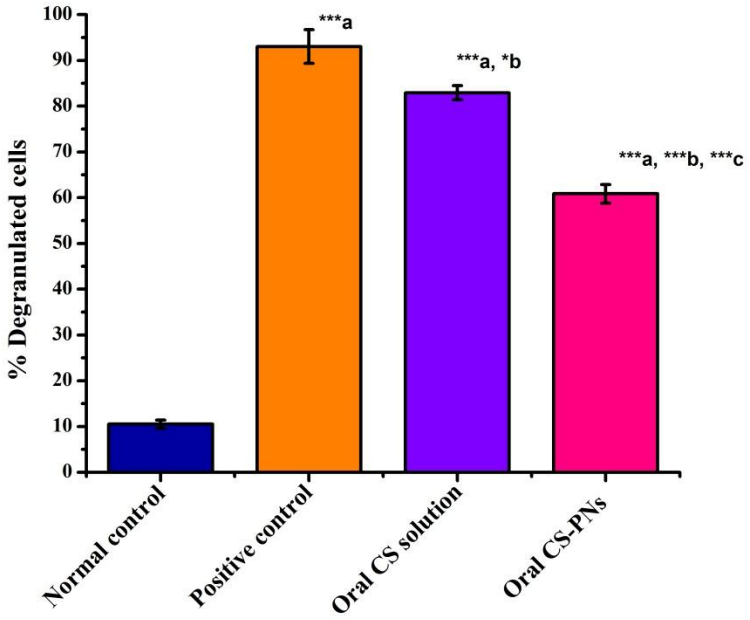


**Figure 5.19 Effect of oral administration of CS solution and CS-PNs on degranulation of peritoneal mast cells in rats (Dose: 20 mg/kg); Vertical bars represent ± SEM; n=6.**

******p*<0.001, *p*<0.05; a *vs* normal control, b *vs* positive control and c *vs* oral CS solution; One-way ANOVA followed by Tukey's multiple comparison test**

Oral administration of CS solution provided ~10.87 % protection against mast cell degranulation compared to positive control and showed 82.92 ± 1.558 % activation after incubation with compound 48/80. However, significantly much higher protection against mast cell degranulation was observed in case of CS-PNs as compared to CS solution ($p$<0.001). Oral administration of CS-PNs provided ~34.58 % protection against mast cell degranulation compared to positive control and showed 60.855 ± 2.017 % activation after incubation with compound 48/80. Additionally, lower amount of histamine release for CS-PNs treated group compared to CS solution

treated and positive control group suggested the better efficacy of CS-PNs for stabilizing the mast cells from compound 48/80 like allergen evoked degranulation [199, 202]. The enhanced efficacy for CS-PNs compared to CS solution after oral administration indicated that CS-PNs would have delivered significantly higher amount of CS in the systemic circulation by improving its GIT permeability and thereby, provided higher protection to the sensitized mast cells against degranulation, which in turn strengthens the findings of *in-vivo* pharmacokinetic study and confirms the hypothesis.

**Table 5.16 Effect of oral administration of CS solution and CS-PNs on compound 48/80 induced degranulation of peritoneal mast cells and histamine release in rats (Dose: 20 mg/kg)**

| Treatment Groups | % degranulated cells | Histamine release (µg/ml) |
|---|---|---|
| **Normal Control** | 10.515 ± 0.881 | 0.033 ± 0.0019 |
| **Positive Control** | 93.033 ± 3.648***[a] | 0.190 ± 0.0083***[a] |
| **Oral CS solution** | 82.920 ± 1.558***[a,*b] | 0.166 ± 0.0043***[a,*b] |
| **Oral CS-PNs** | 60.855 ± 2.017***[a,***b,***c] | 0.120 ± 0.0067***[a,***b,***c] |

*All values reported are mean ± SEM, (n=6). ***p<0.001, **p<0.01; a vs normal control, b vs positive control and c vs oral CS solution; One-way ANOVA followed by Tukey's multiple comparison test.*

### 5.3 Summary

The CS-PNs were successfully prepared by double emulsification solvent evaporation method ($W_1/O/W_2$) with minor modifications. The Plackett-Burman screening design was used for preliminary screening of large number of variables in order to identify critical variables affecting the formulation characteristics of CS-PNs. A 3-level, 3-factor Box-Behnken experimental design was further employed to optimize and to understand the combined influence of screened critical variables (i.e., concentration of

polymer, concentration of surfactant and organic phase/aqueous phase ratio) on physicochemical properties of CS-PNs, i.e., particle size, EE and PDI. The quality by design approach suggested that Box-Behnken experimental design provided a high degree of prediction and realization for optimization of the physicochemical properties of CS-PNs by controlling the different formulation variables. The optimized CS-PNs showed particle size of 262.4 $\pm$ 7.6 nm, EE of 34.26 $\pm$ 1.3 % and PDI of 0.271 $\pm$ 0.02. The optimized batch has desirability of 0.629. The surface morphological and solid state characterizations of optimized CS-PNs pointed towards the encapsulation of CS in an amorphous form inside the spherical shaped polymeric matrix without any physical as well as chemical interactions. *In-vitro* release study of CS-PNs in phosphate buffer pH 7.4 indicated that CS-PNs were able to sustain the drug release up to 24 hr by diffusion controlled process. CS-PNs were physically and chemically stable at different environmental conditions over the period of 6 month. *Ex-vivo* intestinal permeation study demonstrated ~3.98 fold improvements in CS permeation across the intestinal epithelial barrier by forming CS-PNs as compared to pure CS solution. Further, *in-vivo* intestinal uptake study performed using confocal microscopy, after oral administration confirmed the permeation potential of CS-PNs as indicated by their strong green fluorescence. *In-vivo* pharmacokinetic study was performed in rats and revealed ~4.69 fold enhancements in oral bioavailability of CS after its incorporation into nanoparticles as compared to pure CS solution. *In-vivo* mast cell stabilizing activity performed in rats demonstrated significant protection against mast cell degranulation with oral administration of CS-PNs than free CS solution. Conclusively, the developed CS-PNs could definitely be considered as promising delivery strategy for oral pharmacotherapy of CS with greater efficacy.